frontiers | Frontiers in Marine Science

ORIGINAL RESEARCH
published: 14 June 2022
doi: 10.3389/fmars.2022.835260

Characterizing Mesoscale Eddies of Eastern Upwelling Origins in the Atlantic Ocean and Their Role in Offshore Transport

Artemis Ioannou, Sabrina Speich and Remi Laxenaire*

Laboratoire de Météorologie Dynamique LMD-IPSL, Ecole Normale Supérieure, Paris, France

Motivated by the recurrent formation of eddies in the eastern upwelling areas, we examine cross-basin connectivity that is promoted by coherent, long-lived and long-propagating mesoscale eddies in the Atlantic Ocean. By applying the TOEddies detection and tracking algorithm to daily satellite observations (AVISO/DUACS) of Absolute Dynamic Topography (ADT), we characterize mesoscale eddy activity and variability in the North and South Atlantic. This method provides a robust eddy-network reconstruction, enabling the tracking of eddies formed in the Atlantic eastern upwelling systems together with any merging and splitting events they undergo during their lifetime as long as they remain detectable in the altimetry field. We show that during the years of observations, mesoscale eddies are long-lived coherent structures that can ensure oceanic connectivity between the eastern and the western boundaries, as a result of complex inter-eddy interactions. Moreover, alignment of South Atlantic eddies of eastern boundary origins with available Argo floats achieves a mean cross-basin connectivity signal from both anticyclonic and cyc5lonic eddies which is particularly evident at depth, along thermocline isopycnal layers of γ^n = 26 - 27 kg m^{-3}. We explore two individual cyclonic eddy trajectories from *in-situ* measurements gathered by different Argo profiling floats trapped inside the eddy cores. Our results support the hypothesis that mesoscale eddies sustain and transport water masses while subducting during their westward propagation.

Keywords: mesoscale eddies, eastern boundary upwelling systems, oceanic connectivity, cross-basin exchanges, subduction, Agulhas Cyclones

OPEN ACCESS

Edited by:
Regina R. Rodrigues, Federal University of Santa Catarina, Brazil

Reviewed by:
Yuntao Wang, Ministry of Natural Resources, China
Iury T. Simoes-Sousa, University of Massachusetts Dartmouth, United States

****Correspondence:***
Artemis Ioannou
innartemis@gmail.com

Specialty section:
This article was submitted to Physical Oceanography, a section of the journal Frontiers in Marine Science

Received: *14 December 2021*
Accepted: *16 May 2022*
Published: *14 June 2022*

Citation:
Ioannou A, Speich S and Laxenaire R (2022) Characterizing Mesoscale Eddies of Eastern Upwelling Origins in the Atlantic Ocean and Their Role in Offshore Transport. Front. Mar. Sci. 9:835260. doi: 10.3389/fmars.2022.835260

1 INTRODUCTION

Eastern boundary upwelling systems (EBUS) are dynamically complex circulation systems characterized by enhanced mesoscale activity (Correa-Ramirez et al., 2007; McGillicuddy et al., 2007; Stramma et al., 2013; Amos et al., 2019). In the Atlantic Ocean, the Canary Current upwelling system (CCUS) and the Benguela Current upwelling system (BCUS) are among the major EBUS of the world ocean. These areas support highly productive marine ecosystems and sustain significant fisheries (Hutchings et al., 2009; Harvey et al., 2020). Their particular dynamics, influenced by the

combined effect of strong Ekman transport of surface waters and upwelled waters along the coast, give rise to various flow instabilities including the formation of mesoscale eddies (Chaigneau et al., 2009; Chelton et al., 2011; Pegliasco et al., 2015).

Eddies in the CCUS and BCUS are *a priori* expected to be generated by instabilities of the upwelling current fronts (Marchesiello et al., 2003; Marchesiello and Estrade, 2007; Moscoso et al., 2021). Wang et al. (2015, 2021) showed a strong correlation between frontal activity (estimated from Sea Surface Temperature fields) and the variability of alongshore winds. Nevertheless, both upwelling systems have their own specificities and it is difficult to separate the physical mechanisms that are involved in eddy generation. As far as CCUS is concerned, the presence of islands near its upwelling shelf (Canary Islands in the north and Cape Verde in the south) contributes to eddy generation through island-induced mechanisms (Sangrà et al., 2005; Caldeira et al., 2014; Stegner, 2014; Ioannou et al., 2020a; Ioannou et al., 2020b) while downstream of the Gran Canaria, the shedding of both cyclonic and anticyclonic eddies is observed (Arístegui et al., 1994; Arístegui et al., 1997; Basterretxea et al., 2002; Barton et al., 2004; Arístegui and Montero, 2005; Sangrà et al., 2005; Sangrà et al., 2007). On the other hand, high eddy occurrences are found near the African coast (Schütte et al., 2016a) where various instabilities and coastal processes are involved in eddy generation (Dilmahamod et al., 2021). Continuous interactions between island-induced eddies and eddies or filaments from the upwelling have also been reported to entrain nutrient-rich waters further offshore (Arístegui et al., 1994; Arístegui et al., 1997; Basterretxea et al., 2002; Arístegui and Montero, 2005; Sangrà et al., 2005; Sangrà et al., 2007). On the basis of 14 years of satellite observations (1992-2006), Sangrà et al. (2009) have furthermore noted the westward propagation of long-lived eddies from the upwelling. Distinct eddy corridors along which organic matter could be exported into the oligotrophic subtropical gyre in the North Atlantic were documented.

Meanwhile, in the South Atlantic, the BCUS upwelling regime, especially its southern part, is intrinsically bounded to the Agulhas Leakage (Doglioli et al., 2007; Blanke et al., 2009; Veitch and Penven, 2017) that together with the regional circulation, also shapes particularly energetic and dynamically complex local dynamics. The intrusion of warm salty Indian water *via* the spawning of Agulhas Rings from the Agulhas Current retroflection (Arhan et al., 1999; Matano and Beier, 2003; Giulivi and Gordon, 2006; Guerra et al., 2018; Laxenaire et al., 2018; Laxenaire et al., 2019; Laxenaire et al., 2020), along with the BCUS dynamics as well as the complex bathymetry in the Cape Basin (Matano and Beier, 2003), causes strong interactions between cyclonic and anticyclonic eddies (Boebel et al., 2003; Richardson and Garzoli, 2003; Giulivi and Gordon, 2006; Souza et al., 2011). Numerous eddies with high cyclonic versus anticyclonic ratios are observed, (3:2 in favor of cyclones (Boebel et al., 2003)), while various exchanges and water-mass modification processes take place (Rusciano et al., 2012). Indeed, satellite imagery has revealed the strong influence of the Agulhas Rings in the Cape Basin that may also entrain and export cold upwelling waters along their pathway beyond the upwelling shelf (Duncombe Rae et al., 1992). Yet there are only a few studies (Giulivi and Gordon, 2006; Arhan et al., 2011; Souza et al., 2011) that emphasize on the role of cyclonic eddies from the upwelling and their dynamical characteristics. During a recent hydrographic transect along 34.5°S, an Agulhas cyclone originated from an instability along the Benguela upwelling system has been observed near the Southern Africa shelf (Manta et al., 2021). Vessel Mounted Acoustic Doppler Profiler (VM-ADCP) measurements revealed intense velocities for the cyclone that reached 80 cm/s at 100 dbar. Strong temperature anomalies extended between 100 - 700 dbar.

Generally however until now, with the sole exception of the multi-year observations reported in Sangrà et al. (2009), the characterization of eddies with upwelled origins has been surveyed only occasionally and open questions are still raised on how far such eddies may travel in the Atlantic Ocean. Unlike waves, coherent eddies, characterized by rotational speeds greater than their translating motion (Flierl, 1981; Chelton et al., 2011; Polito and Sato, 2015), can trap water masses in their cores for long periods and remain physically isolated from outside perturbations while propagating. Sparse yet significant observations made *via* Argo floats that stayed trapped inside eddies for significant time periods (Ioannou et al., 2017; Guerra et al., 2018; Laxenaire et al., 2018; Laxenaire et al., 2019; Nencioli et al., 2018) confirm the existence of such long-lived and long-propagating eddies.

Combined hydrographic observations in the CCUS (Basterretxea et al., 2002; Brandt et al., 2015; Schütte et al., 2016a; Schütte et al., 2016b; Karstensen et al., 2017) have pointed out that upwelled eddies may substantially contribute to the global offshore transport of properties. Given that eddies inhibit lateral exchanges with the outside environment, they may be responsible for the gradual development of anoxic environments within their cores (Brandt et al., 2015; Schütte et al., 2016b; Karstensen et al., 2017). Eddy-resolving numerical models (Gruber et al., 2011; Nagai et al., 2015) have shown that such eddies can act as the main exporters of nutrients and biological components out of coastal areas. Subduction of upwelling filaments is also suggested as a possible mechanism contributing to the offshore transport of upwelled waters affecting biological productivity by moving phytoplankton and nutrients in or out the euphotic zone. In other upwelling systems, their contribution to the offshore transport of nutrient- and carbon-rich coastal waters has also been highlighted (Amos et al., 2019). In the global ocean, increased chlorophyll concentrations have been continuously reported within eddies (McGillicuddy et al., 2007; Lehahn et al., 2011; Villar et al., 2015; Dufois et al., 2016; Cornec et al., 2021a; Cornec et al., 2021b). Mesoscale eddies may thus significantly alter the distribution of properties along their propagation. Further characterization and quantification of eddies shed from upwelling areas is therefore crucial in order to deepen our understanding of cross-shore export of properties, the dynamical processes shaping local marine ecosystems and marine connectivity.

Satellite altimetry remains a powerful tool for characterizing the ocean mesoscale. Despite its various limitations and uncertainty (Amores et al., 2018; Laxenaire et al., 2018; Stegner et al., 2021), the development of automatic eddy detection algorithms has made the characterization of eddies from satellite altimetry an easier task, allowing them to be quantified and their temporal variability followed over long time periods. Automatic detection and tracking algorithms can thus identify eddies *via* their imprints on sea surface height, locate their centers and quantify their main horizontal dynamical parameters such as size, intensity, surface geostrophic velocity, drifting speed, etc. Recent techniques (Li et al., 2014; Le Vu et al., 2018; Laxenaire et al., 2018; Cui et al., 2019) now also provide methods to identify merging and splitting events. In this study, we use the TOEddies Global Atlas to detect and follow eddies in the Atlantic Ocean, building on the approach taken by Laxenaire et al. (2018) to investigate the Agulhas Rings in particular. The TOEddies Atlas not only provides information on eddy dynamical characteristics together with their merging and splitting events, but also reconstructs a complex eddy network, linking eddy trajectories associated with the merging with other eddies or the splitting into two or more eddies. TOEddies is among the few algorithms that has been qualified against an independent dataset, with eddies derived from surface drifter trajectories and dubbed as "loopers" (Lumpkin, 2016). Moreover, in recent years TOEddies has successfully aided the positioning and tracking of eddies in near-real time during several oceanographic cruises (Manta et al., 2021; Stevens et al., 2021). The TOEddies Atlas furthermore incorporates available colocalized vertical information from Argo floats with its eddy detection (Laxenaire et al., 2018; Laxenaire et al., 2020). This combination of satellite altimetry with autonomous measurements has been proven especially useful for analyzing the vertical properties of eddies (Chaigneau et al., 2011; Pegliasco et al., 2015; de Marez et al., 2019; Laxenaire et al., 2019; Laxenaire et al., 2020)

Indeed, vertical information on eddies offers to shed valuable light on their structure and behavior. For example, Pegliasco et al. (2015), through comparisons of the surface and subsurface characteristics of long-lived eddies originating from four of the major EBUS in the global ocean, found a high percentage of anticyclonic and cyclonic eddies to be subsurface-intensified. Surface-intensified eddies that experience summer restratification can potentially separate from the surface, becoming subsurface-intensified eddies and retaining a homogeneous water layer in their core. Such "mode-water"eddies, as they are called in the scientific literature, have been surveyed in the Canary upwelling system (Schütte et al., 2016a; Schütte et al., 2016b; Karstensen et al., 2017; Dilmahamod et al., 2021) and in the Cape Basin (Laxenaire et al., 2019; Laxenaire et al., 2020). Karstensen et al. (2017) surveyed an anticyclonic mode water eddy reporting low oxygen in its eddy core that originated from the Mauritanian upwelling region. Barceló-Llull et al. (2017) also discussed a subtropical intrathermocline four-months-old anticyclonic eddy in the Canary eddy corridor in 2014. In the south Atlantic, Laxenaire et al. (2019, 2020) found that Agulhas Rings subside gradually in deeper ocean layers, transforming in subsurface-intensified eddies along their westward propagation. This transition is associated with an important decrease in their surface imprint on altimetry maps and other properties such as sea surface temperature and salinity. Even if the surface signal of such eddies attenuate over time, the reconstructed eddy vertical structure shows no significant changes. The intense heat loss that these eddies experience at the Agulhas Current retroflection and during their displacement in the southern Cape Basin area can lead to significant cooling and increased density of the rings' upper 400-600 m layers (Arhan et al., 2011). As a result, a subsidence transition from surface to subsurface eddies occurs while drifting westward and encountering the warmer South Atlantic subtropical gyre waters (Laxenaire et al., 2019; Laxenaire et al., 2020). This transition to subsurface introduces a new challenge when identifying mesoscale eddies from satellite observations as the altimetric signal can capture as well as surface-intensified eddies and subsurface-intensified ones (Assassi et al., 2016; Dilmahamod et al., 2018; Laxenaire et al., 2020). Also, when the eddy signal disappears from altimetry maps, this is very likely not due to the eddy's dissipation but to its increased penetration at depth.

In this paper, we examine the contribution of mesoscale eddies with origins in the EBUS to the offshore export, transport and distribution of properties in the Atlantic Ocean. Our approach consists in characterizing the horizontal and vertical extent of mesoscale eddies with a combination of satellite altimetry and Argo floats measurements using the TOEddies Atlas (Laxenaire et al., 2018; Laxenaire et al., 2020). We focus on the two major eastern boundary upwelling systems of the Atlantic Ocean, namely the Benguela Current upwelling system (BCUS) and the Canary Current upwelling system (CCUS), that are characterized by enhanced mesoscale activity. We thus explore the oceanic connectivity that is potentially promoted by coherent, long-lived and long-propagating mesoscale eddies across basins.

The paper is organized as follows: in section 2 we describe the various datasets that we used, with an overview of the TOEddies Dynamical Atlas and the available Argo float measurements. Section 3, presents the dynamical characteristics of eddies in the Atlantic Ocean and in the upwelling systems considered in this study. We then discuss the mean horizontal and vertical structure of oceanic connectivity that is achieved by mesoscale eddies of eastern upwelling origins. We also present two cyclonic eddies that were sampled by a high number of vertical profiles over a one-year period along their dynamical evolution in the South Atlantic. Finally our results are summarized in section 4.

2 DATA AND METHODS

2.1 TOEddies Global Dataset and Argo Profiles Co-Location

To characterize mesoscale eddies, we used the TOEddies Global Atlas dataset (Laxenaire et al., 2018) that provides daily eddy

detection and tracking from satellite observations of Sea Surface Height (SSH), over a 24-year period from 1993 to 2018. The TOEddies Global Atlas is applied on fields of Absolute Dynamic Topography (ADT) that are projected on a $\frac{1}{4}°$ ($dX \simeq 25\,km$) all-sat-merged dataset and distributed by AVISO/DUACS.

Firstly, eddies are identified by TOEddies as points of extreme ADT. ADT fields are chosen over Sea Level Anomaly (SLA) fields even though the latter have been widely used (Chelton et al., 2011; Cui et al., 2019; Tian et al., 2019), since SLA fields represent a deviation of SSH from a temporal SSH mean and potentially lead to misinterpretations of the eddy signals (Pegliasco et al., 2020). Next, closed contours of SSH that exceed an eddy amplitude threshold, delimit the eddy outer boundary. Once the eddy outer boundary is identified, the SSH contour of maximum azimuthal speed V_{max} is also detected. The latter delimits the eddy dynamical core that physically remains uninterrupted by lateral exchanges with the environment. The outer $\langle R_{out} \rangle$ and characteristic radius $\langle R_{max} \rangle$ of an eddy can be then estimated. The mean radii will correspond to the same area as that of a circular disc would have when enclosed by the characteristic and the outer contour respectively. In this study, we mainly use R_{max} and V_{max} to quantify the eddy size and the intensity respectively.

To follow eddies over time, TOEddies requires eddy areas to overlap between successive time steps. This overlapping criterion is additionally combined with a cost-function that takes into account dynamical characteristics such as the eddy size, intensity and distance (Laxenaire et al., 2018; Le Vu et al., 2018) in order to reconstruct the eddy trajectories when eddies split or merge. This technique allows the identification of unique segments of eddies rather than eddy occurrences. Eddies that interact with each other, either by a merging or a splitting event, are assigned orders of interactions and can be tracked in the AVISO time-series. In this way, the TOEddies algorithm reconstructs a complex eddy network and enables the tracking of eddies of specific origins (Laxenaire et al., 2018). The accurate detection of merging and splitting events is necessary as successive eddy-eddy interactions can alter the main eddy pathways and impact the reconstruction of eddy trajectories (Du et al., 2014; Li et al., 2014; Le Vu et al., 2018; Cui et al., 2019).

Moreover, TOEddies combines its derived daily eddy detection with vertical information on temperature and salinity from autonomous Argo floats measurements over the period 2000-2017. For this study, we restricted our analysis to the Atlantic Ocean (80°W-30°E and 60°S-60°N) and around ~ 25% of the total colocalisation dataset corresponding to 276,259 individual Argo profiles of temperature and salinity collected by 3,024 different floats. The spatial distribution of available profiles in the North and South Atlantic is shown in **Figure S1**. For each profile, temperature and salinity were converted to potential temperature and absolute salinity using TEOS-10 (McDougall and Barker, 2011). Potential density σ_θ and neutral density γ^n profiles were also estimated. To reconstruct the hydrography of the "no-eddy" environment around a given position and a given date, Argo profiles were separated in two groups: those detected inside mesoscale eddies by TOEddies, or outside of them (outside the last eddy contour). The latter were considered to sample the environment and are used to construct climatological profiles of T, S and σ in the given area. Thus, the "no-eddy" climatology consists of all profiles located outside of eddies at a radial distance ≤1° around the selected position and during a ±30 day period from the given date (regardless of the year) over the 17 years.

We further limited our selection of Argo floats that were located inside eddies from the different eddy network reconstructions that are considered in this study (see subsection 3.3). To analyze mean vertical properties of the eddy networks, we grouped profiles in 1° × 1° bins. For each bin and at each depth level, we computed the mean characteristics of temperature and salinity as well as their corresponding anomalies with respect to the climatology. Mean properties were also analyzed at different sigma levels by interpolating all properties to constant density layer intervals ($\Delta\sigma_\theta$ = 0.01 kg m^{-3}).

2.2 Sea Surface Temperature and Atmospheric Data

We used the ERA-Interim data-set to compute the seasonal and interannual variations of wind forcing and sea surface temperature for the upwelling areas. This reanalysis provided the atmospheric fields at $\frac{1}{4}°$ spatial resolution and temporal resolution of 1 h. Sea surface wind components at 10 m and sea surface temperature were obtained from the ERA-Interim synoptic fields from 1993 to 2018 (Hersbach et al., 2018). Wind stress components and the wind stress curl were calculated with the standard bulk formula $[\underline{\tau} = \rho_{air} C_D V_{wind} \underline{V_{wind}} (Nm^{-2})]$ = with ρ_{air} = 1.25 kg m^{-3} and a constant C_d coefficient (C_d = 1.6 10^{-3}). We considered four different upwelling subsystems, separating the CCUS and BCUS into two sub-systems in the North (nCCUS and nBCUS) and the South (sCCUS and sBCUS) as discussed further in section 3.2 (**Figure 6**). We built the monthly mean estimates of wind forcing and sea surface temperature for the different subsystems and compared their temporal variability.

3 CHARACTERIZATION OF MESOSCALE EDDIES IN THE ATLANTIC OCEAN

3.1 Mesoscale Activity in the Atlantic Ocean

The TOEddies dynamical dataset detects and tracks more than 14,169,103 eddies (with lifetimes of at least 7 days) and 408,202 eddy trajectories in the Atlantic Ocean.

To characterize mesoscale eddy activity, we present in **Figure 1**, separately for cyclones and anticyclones, histograms of eddy lifetimes, characteristic radii and velocities. Histograms of eddy dynamical characteristics are shown separately for the North and South Atlantic. In these diagrams we have filtered out mesoscale eddies with radius smaller than ≤ 18 km, in order to avoid small-scale features that are not accurately captured by

altimetry. We find an almost equal percentage of cyclonic and anticyclonic eddies with lifetimes exceeding 16 weeks even if cyclones are slightly higher in number than anticyclones (cyclonic eddies represent 51.7% of the total for the North and 53.1% for the South Atlantic). Around 57% of the tracked eddies were detected in the North Atlantic. In total, eddies with lifetimes less than 4 and 16 weeks respectively represent almost 75% and 95% percentile of the eddy lifetime distribution as provided by satellite altimetry maps (**Figures S2, S9**) On average, we detected cyclonic eddies with lifetimes more than 16 weeks to have slight smaller radii (by 3%) than anticyclones in both hemispheres, while their characteristic velocities exceeded that of the anticyclones, mostly in the North Atlantic, by 14%.

Figure 2 shows trajectories of mesoscale eddies in the Atlantic ocean as tracked by TOEddies. Eastward versus westward trajectories were identified by estimating their net displacement between their first and last position. Eastward propagating eddies with lifetimes ≥16 weeks accounted for only 17.5% of the total trajectories and they corresponded mainly to eddies tracked in the Antarctic Circumpolar Current (ACC) and in the subpolar North Atlantic (north of 40°N) (**Figure 1**). In line with previous studies (Chelton et al., 2011), the majority of long-lived eddies in the North and South Atlantic were found to propagate westward influenced by the β-effect (**Figure 2** shows westward eddies with lifetimes ≥52 weeks). The total number of westward-propagating eddies in the North Atlantic was higher than the ones of the South Atlantic (representing 59% of the total westward trajectories).

Eddy trajectories were also sorted on the basis of their estimated lifetimes in **Figure 3**. The ratio of cyclone versus anticyclone lifetimes was similar only for eddies with lifetimes of less than 52 weeks (**Figure 1** and **Figures S2B, C**). In agreement with previous findings (Chelton et al., 2011; Tian et al., 2019), eddies with longer lifetimes (≥52 weeks, approximately 1.5 years) were mostly anticyclonic (**Figures S2**). In the South Atlantic, around 60% of eddy trajectories were indeed anticyclonic, while in the North Atlantic the percentage of eddies of both polarities remained close (51% anticyclonic over 49% cyclonic). Nevertheless, the TOEddies algorithm detected a higher number of long-lived cyclones originating in the upwelling systems of both hemispheres.

Figure 4 compares the cumulative number of Atlantic mesoscale eddy first (A, B) and last detections (C, D) as well as eddy-eddy interactions (merging and splitting events) (E, F) computed on a 1° × 1° gridded map as detected daily during the study period (1993 - 2018). In order to account for all possible eddy-eddy interactions, we counted centroids of eddies that were tracked for at least 4 weeks. Hot spots of eddy activity were characterized by high density of eddy generations exceeding $N > 30$ eddies per degree square. We found a higher rate of eddy generation near the eastern boundary of the ocean basin and, in particular, within the major eastern upwelling boundary systems (Canary in the North and Benguela in the South Atlantic) as well as within the western boundary currents (Brazil Current in the South Atlantic and the Gulf Stream in the North Atlantic).

Several areas where eddies were frequently generated were also areas where eddies disappeared from altimetry maps. Nevertheless, the difference on average between generation and termination points (not shown here) consists mostly of areas favorable for the generation of eddies. We noted that high spatial distribution of merging and splitting events also occurred in similar places, a fact that emphasizes the importance of accounting for eddy-eddy interactions to provide a complete dynamical description of the evolution of detected eddies. Merging and splitting events in the North Atlantic involved 53% of cyclonic eddies while in the South Atlantic a similar percentage of 54% was associated with interactions between anticyclonic eddies.

Areas of strong mesoscale activity are usually identified by estimating their eddy kinetic energy (EKE). Similarly to Chelton et al. (2011), we computed the total kinetic energy (KE) from the geostrophic velocity fields as derived from the daily ADT maps, namely by subtracting the temporal mean of the velocity geostrophic components over the study period

$$KE = \frac{1}{N}\sum_{i=1}^{N}(u(x,y,t) - \bar{u}(x,y))^2 + (v(x,y,t) - \bar{v}(x,y))^2 \quad (1)$$

where $\bar{u} = \frac{1}{N}\sum_{i=1}^{N}u(x,y,t)$ and $\bar{v} = \frac{1}{N}\sum_{i=1}^{N}v(x,y,t)$. Based on TOEddies daily eddy detection, we were further able to distinguish the percentage of EKE attributed only to anticyclonic and cyclonic eddies respectively, and thus recover areas of eddy kinetic energy associated only with mesoscale eddy activity. This is achieved with a delta function $\delta(x, y, t)$ set to zero when the KE lay outside the last eddy contour and 1 when inside

$$EKE = \frac{1}{N}\sum_{i=1}^{N}((u(x,y,t) - \bar{u}(x,y))^2 + (v(x,y,t) - \bar{v}(x,y))^2)\delta(x,y,t) \quad (2)$$

We plotted in **Figure 5**, the ratio of eddy kinetic energy versus total kinetic energy separately for cyclonic and anticyclonic eddies. The eastern upwelling areas are among the most energetic areas in the Atlantic Ocean. In the CCUS upwelling areas, the signatures of both cyclonic and anticyclonic eddies contribute to this eddy kinetic energy. In the BCUS, strong KE signal are mostly associated with cyclonic eddies near the upwelling areas, while the intense Agulhas eddy contribution to KE is visible in the right panel of **Figure 5**.

3.2 Dynamical Characteristics of EBUS Trajectories

The mean statistical properties of all the eddies detected by TOEddies in the Atlantic Ocean show that the EBUS represent areas of increased eddy density due to frequent eddy generations, interactions as well as high EKE. In particular, several long-lived and long-propagating eddies were found to originate from the EBUS.

To investigate the eddies' role in greater detail, we firstly defined eddies originating from the upwelling systems as those

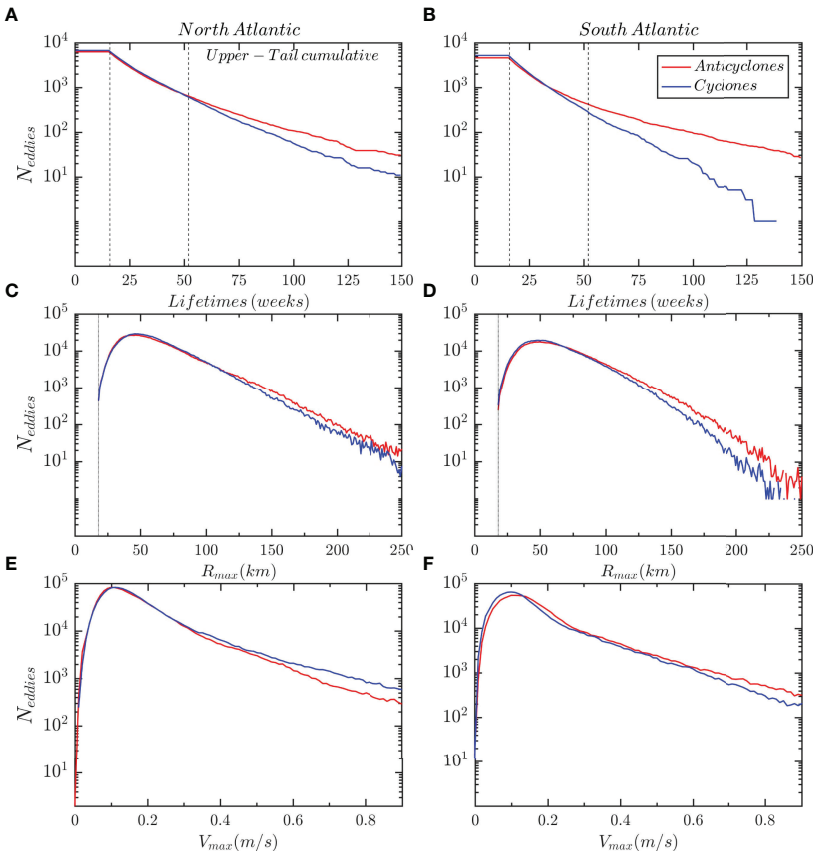

FIGURE 1 | Upper-tail cumulative histograms of eddy lifetimes (weeks) **(A, B)** and histograms of eddy characteristic radius R_{max} (km) **(C, D)** and velocity V_{max} (m/s) **(E, F)** of anticyclonic (red colors) and cyclonic eddies (blue colors) for the North (left panels) and South (right panels) Atlantic Ocean during the 1993-2018 period. We consider only mesoscale eddies having lifetimes ≥ 16 weeks and characteristic radii larger than R_{max} ≥ 18 km as indicated by the dashed lines in panels **A**–**D** respectively.

initially detected within the BCUS and CCUS regions before propagating into the Atlantic Ocean. To represent the upwelling fronts and broadly capture eddies generated from shelf's instabilities, we chose the 4,000 m isobath. In accordance with previous studies (Cury and Shannon, 2004; Desbiolles et al., 2014; Ndoye et al., 2014), we additionally divided the BCUS upwelling system into two subsystems: the north and south upwelling cells (nBCUS and sBCUS) at approximately 26.5°S near Lüderitz. This south and north division has been reported to be distinct in terms of climatological wind conditions and regional frontal dynamics (Wang et al., 2015; Wang et al., 2021) but also in terms of biological clustering (Blamey et al., 2015; Kirkman et al., 2016). A similar north and south division was made for the CCUS at around 20°N near Cape Blanc (nCCUS and sCCUS) (Barton et al., 1998; Benazzouz et al., 2014; Pelegrí and Benazzouz, 2015). The different upwelling subregions are indicated in **Figure 6** in different colors (blue for the north and green for the south).

In **Figures 6A, B** and **E, F** we display the eddy trajectories originating from the different subsystems that could be tracked from satellite altimetry maps for more than 16 weeks during the 1993-2018 period. Taking all eddy trajectories into account, both cyclonic and anticyclonic eddies were found to populate the upwelling subregions. In total numbers, TOEddies tracked more eddies originating from the CCUS subsystems than from the BCUS while the highest number of individual eddy trajectories was found for the nCCUS. The number of tracked cyclones was consistently higher than that of the anticyclones with the nCCUS being the only subsystem to be populated by an equal mixture of eddy types (50% cyclones/49% anticyclones). The asymmetry between cyclonic and anticyclonic eddies was the strongest for the sBCUS where 83% of the eddies are cyclonic. Slightly lower percentage (67%) was found for the sCCUS, while cyclonic eddies originating from the nBCUS were almost double the number of the anticyclonic ones. These findings are in line with previous observations (Boebel et al., 2003).

Moreover, eddy generation can vary considerably from year to year (**Figures 6C, G**). On average, in the sCCUS, the rate of cyclonic eddy generation was close to 8 ± 1.8 eddies per year (lifetimes ≥ 16 weeks in **Figure S4**). Stronger interannual variations with an average rate of 7.7 ± 2.6 cyclones/year were found for the sBCUS. In the nBCUS, this rate was estimated close to 5.3 ± 1.7 cyclones/year. Anticyclonic and cyclonic generation in the nCCUS yielded similar rates, close to 8 ± 2

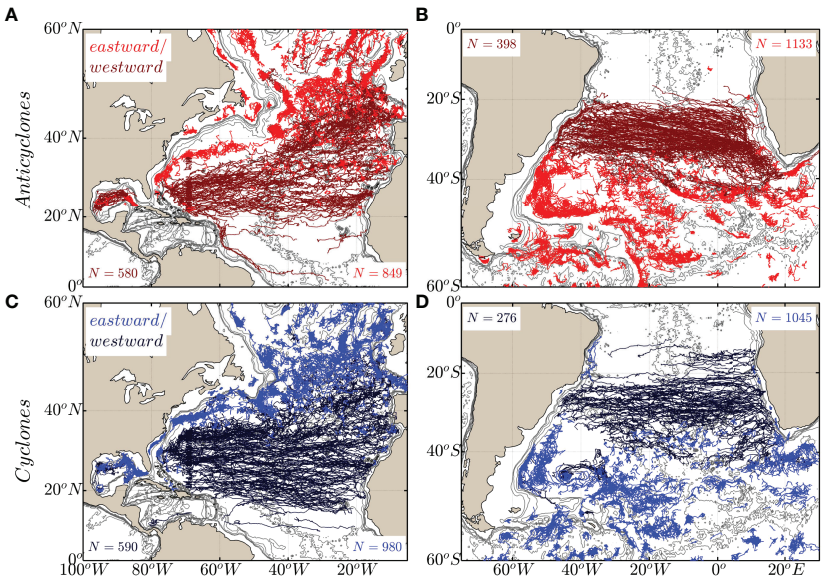

FIGURE 2 | Trajectories of eastward (lighter colors) versus westward (darker colors) propagating eddies with lifetimes longer than ≥16 weeks and ≥52 weeks respectively. Anticyclonic **(A, B)** and cyclonic **(C, D)** are indicated by blue and red, as detected *via* the TOEddies algorithm over a 24-year period (1993-2018). Bathymetry shallower than 4,000 m is indicated by gray lines.

eddies/year. Conversely, anticyclonic generation rates were consistently lower in the other systems: below 4.2 ± 1.8/year for the sCCUS, 2.8 ± 1.2/year for the nBCUS and 1.9 ± 1/year for the sBCUS.

During specific years, eddies originating from the Atlantic EBUS were tracked for longer periods of time while propagating westward. After generation, cyclones from the sCCUS and nCCUS mainly translated westward and north-westward, while anticyclones followed very different trajectories and tended to propagate south-westward. Meanwhile, cyclones generated in the nBCUS and sBCUS mainly translated westward and south-westward, towards the southern branch of the South Equatorial

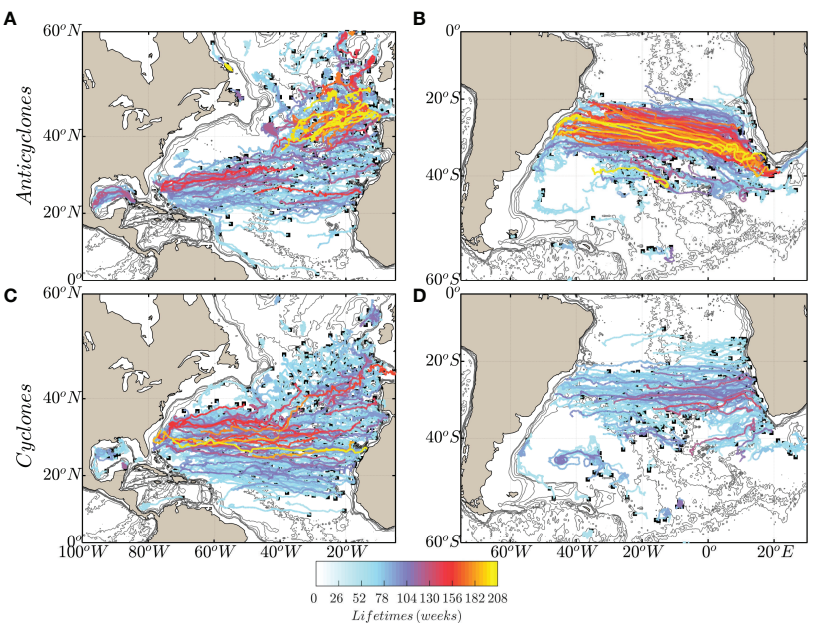

FIGURE 3 | Trajectories of anticyclonic **(A, B)** and cyclonic **(C, D)** eddies as detected *via* the TOEddies algorithm over a 24-year period (1993-2018) having a lifetime longer than ≥ 52 weeks. Each trajectory is colored on the basis of their estimated lifetimes (weeks). Bathymetry shallower than 4,000 m is indicated by gray lines.

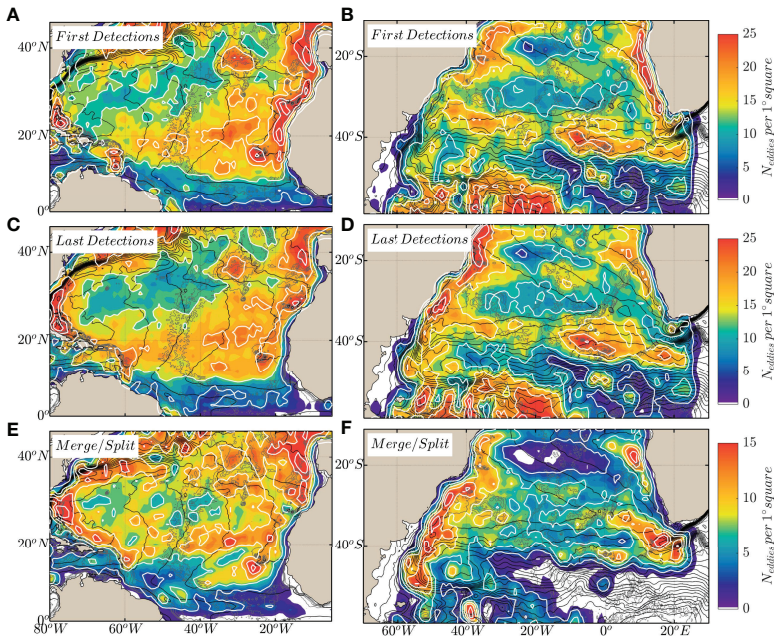

FIGURE 4 | Frequency maps of first (panel **A**, **B**), last (panel **C**, **D**) detection points and merging and splitting points (panel **E**, **F**) of mesoscale eddies with lifetimes longer than ≥ 4 weeks as detected in the South and North Atlantic from the TOEddies global Atlas over a 24-year period (1993-2018) gridded over 1° × 1° bins (smoothed using a 1° × 1° window). The mean dynamic topography (MDT in cm) is shown by black contours and bathymetry shallower than 4,000 m depth by gray lines.

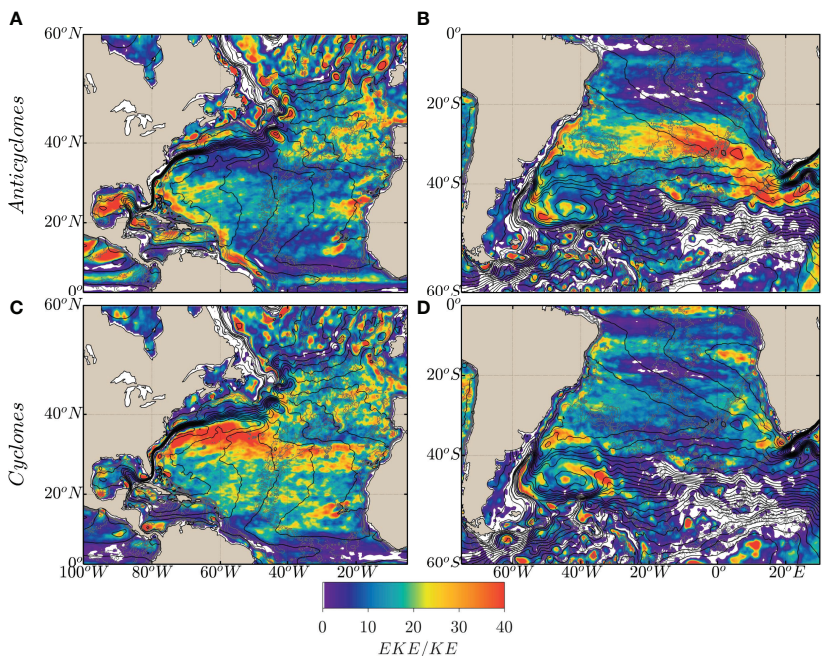

FIGURE 5 | Ratio of the contribution of mesoscale eddy kinetic energy (EKE) to the total kinetic energy (KE) in the North (left panels) and South Atlantic (right panels), respectively for anticyclonic **(A, B)** and cyclonic **(C, D)** eddies gridded over 1° × 1° bins. The mean dynamic topography (MDT in cm) is shown by black contours and bathymetry shallower than 4,000 m depth by gray lines.

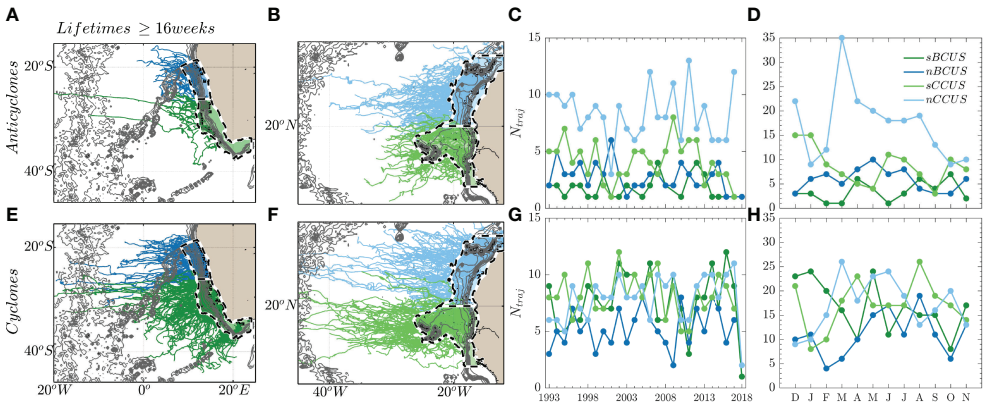

FIGURE 6 | Eddy trajectories originating from the four upwelling subsystems: nBCUS and sBCUS **(A, E)** and sCCUS and nCCUS **(B, F)** as obtained from TOEddies Global Atlas with lifetimes more than ≥ 16 weeks. The mean annual and monthly number of eddies are indicated in panels **C**, **G** and **D**, **H** respectively for anticyclonic and cyclonic trajectories. The north and south upwelling regions of the BCUS and CCUS are indicated by the blue and green patch areas respectively.

Current (Majumder et al., 2019; Luko et al., 2021). Thus, equatorward/poleward deflections for anticyclones/cyclones respectively were also confirmed here in agreement with previous findings (Morrow, 2004; Chaigneau et al., 2009; Chelton et al., 2011; Schütte et al., 2016a). Among these long-lived mesoscale eddies, several stood out with lifetimes exceeding 2 years and propagation distances exceeding 2,000 km (**Figure S5**).

If we assume that eddy generation in the BCUS and CCUS is mainly driven by instabilities of the upwelling thermal front, we can then expect their formation to be associated with the upwelling seasonal variations. We therefore explored the seasonal variations of different indices for the four Atlantic EBUS subsystems examined in the present study (see **Supplementary Material Figures S6, S7**). The mean monthly variations of all upwelling indicators showed the nCCUS and nBCUS upwelling subregions to exhibit a permanent upwelling regime while the sCCUS and sBCUS subregions undewent a marked upwelling seasonal cycle (Benazzouz et al., 2014; Pelegrí and Benazzouz, 2015; Brandt et al., 2015).

Even if mesoscale eddies are expected to form more frequently when the upwelling seasonal variations are the strongest, we found that eddy generation does not exhibit marked seasonal variations (**Figure 6**). Moreover, when a seasonal cycle is detectable in the eddy generation, it does not always coincide with an intenser upwelling seasonal phase (**Figure S6**). For instance, in the nCCUS, cyclonic and anticyclonic eddy generation peaks in March just after the maximum SSTa (Sea Surface Temperature anomaly) that peaks during winter (November/December). Similarly, in the sCCUS cyclonic eddy generation peaks in August, a period of weak upwelling intensity. On the other hand, in the sBCUS, cyclonic eddy generation peaks in May, at the end of the most intense upwelling season, when the SSTa is at its minimum (**Figure S6D**). In the nBCUS, increased cyclonic eddy generation is observed from February till May (peak in May for AEs), a fact that could be associated with the minimum SSTa during May. Nevertheless, the maximum number of CEs is observed during August, which is out of phase with any upwelling index considered (SSTa or WSCa,- (**Figures S6D, E**). Even though we have found no direct correlation, we suspect that eddy generation in the upwelling regions is controlled by nonlinear processes involved. For instance, Marchesiello et al. (2003) have shown mesoscale eddy variability in the California current system to be linked with alongshore current instabilities. Marchesiello and Estrade (2007) have further demonstrated that stratification and topography alone can substantially affect the available potential energy initially provided by regional wind forcing. This suggests that more thorough investigations are necessary to understand the connections between regional forcing and eddy generation.

In **Figure 7**, we compare the mean horizontal characteristics of the eddies from the four upwelling subsystems. Histograms of eddy characteristic radii and velocities were plotted separately for cyclonic and anticyclonic eddies. Eddy lifetimes longer than 16 weeks were considered. In the nBCUS and nCCUS, the characteristic radii of cyclonic eddies were estimated at $\langle R_{max} \rangle$ = 67.1 ± 23 km and $\langle R_{max} \rangle$ = 59.4 ± 21 km, 13% and 5% larger than the equivalent average radius of the anticyclones. We found similar sizes (66.3 ± 23 km) for sCCUS cyclones and anticyclones. Cyclones originating from the sBCUS had a mean size of $\langle R_{max} \rangle$ = 63.4 ± 22 km. These were the most intense eddies among the four upwelling systems with mean characteristic velocities reaching almost $\langle V_{max} \rangle$ = 30 ±19 cm/s, which was twice those of the sCCUS cyclonic eddies (14 ± 7 cm/s), nCCUS (14 ± 15 cm/s) and nBCUS (12 ± 6 cm/s). We noted that the mean horizontal characteristics of eddies from the upwellings were associated with large standard deviations indicating that eddy sizes and intensities could vary substantially among the years of observations.

To investigate the mean vertical structure of eddies from each subsystem, we further investigated certain long-lived trajectories of **Figure 6**, limiting ourselves only to those that were additionally

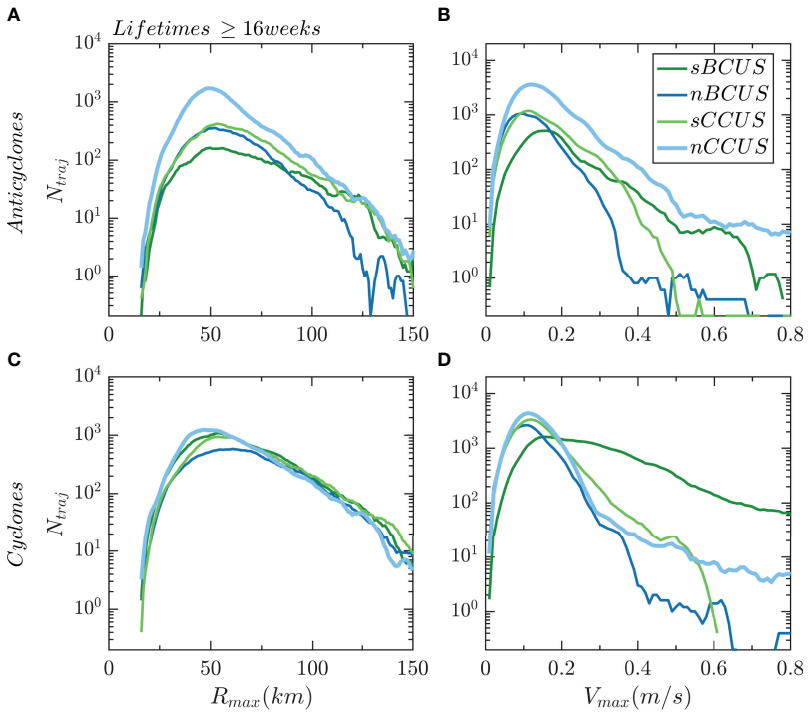

FIGURE 7 | Histograms of eddy characteristic radii R_{max} (km) and velocities V_{max} (m/s) for anticyclonic **(A, B)** and cyclonic **(C, D)** trajectories originating from the different upwelling subsystems considered in this study (lifetimes ≥ 16 weeks).

sampled by at least 1 Argo float at a radial distance smaller than or equal to the eddy characteristic radius ($d_{argo} \leq R_{max}$). **Figure 8** shows the mean vertical structure of temperature and density anomalies of AEs and CEs from each upwelling subsystem. On average, the CEs presented larger anomalies than the AEs. Moreover, BCUS cyclones seemed to contain waters from the environment colder by -1.76°C in the sBCUS and by -1.22°C in the sBCUS in comparison with cyclones from the CCUS whose anomalies remained below 1°C (-0.46°C and -0.7°C in the sCCUS and nCCUS). On average, CCUS eddies displayed shallower vertical extents, occupying mostly shallower and less dense layers (γ^n = 25.2 - 27.1 kg m^{-3}) in comparison with eddies from the BCUS that extended further deeper at higher density intervals (γ^n = 26.5 - 27.14 kg m^{-3}). CEs in the sCCUS were characterized by the shallower vertical extent (γ^n = 25.96 kg m^{-3} ~ 70 m depth) in comparison with CEs from the sBCUS whose maximum anomaly in temperature centered at γ^n = 27.07 kg m^{-3} and at almost 430 m depth. It should be pointed out that all above properties were derived from Argo floats that sampled eddies of the upwelling subregions at different radial distances, while always remaining inside the eddy dynamical core. This selection was made in order to retain a relatively large number of Argo floats for each subregion ($N_{Argo} \geq 20$), in our calculation of the estimated mean EBUS vertical properties. Nevertheless, when taking into account floats located at distances close to the eddy center ($d_{argo} \leq$ 0.5 R_{max}), we found that the mean eddy hydrological anomalies intensified by at least 30% (even growing to 60% for the sBCUS and sCCUS subregions). Accordingly, we suggest that the distance from the eddy center should be taken into further consideration when investigating its impact on nutrient or chlorophyll distribution (Wang et al., 2018).

3.3 Mean Upwelled Eddy Connectivity Signal

The main exporters of nutrient-rich waters from the CCUS and BCUS seem to be mostly associated with cyclonic features. Apart being areas of frequent eddy generation these EBUS are also associated with large eddy-eddy interactions that lead to numerous eddy splitting and merging events (**Figure 4**). Such events alter the main eddy pathways and are supposedly linked with significant transfers of waters. It is hence essential to identify merging and splitting events of both eddy types in order to understand the evolution of eddies.

Following Laxenaire et al. (2018), we reconstructed an eddy network comprising all trajectories related with various filiations to eddies of upwelled origins. By assigning the order of eddy-eddy interactions, the resulting eddy trajectories network assembles all eddies connected *via* merging or splitting and traces them from the upwelling areas further offshore in the Atlantic. **Figure 9** shows the eddy-network reconstruction for the two key areas the BCUS and the CCUS upwelling systems. Trajectories indicated in black are the reference trajectories that originated from the shelf and are assigned an order zero. The order number increases in relation to the number of interactions that are needed to trace back or forward to a reference trajectory.

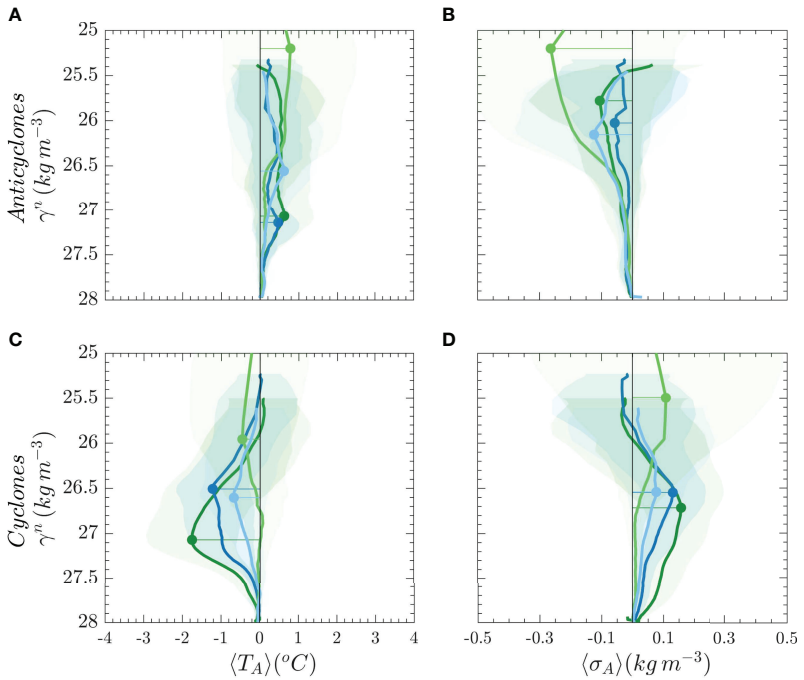

FIGURE 8 | Mean temperature $\langle T_A \rangle$ (°C) and density $\langle \sigma_A \rangle$ (kg m^{-3}) anomalies as derived from Argo profiles tracked inside anticyclonic **(A, B)** and cyclonic trajectories **(C, D)** with lifetimes more than ≥ 16 weeks originating from the different upwelling subsystems considered in this study. Only Argo profiles located at a radial distance of less than R_{max} from the estimated eddy center were kept ($d_{argo} \leq R_{max}$).

In total, the BCUS and the CCUS eddy networks were composed of 11,764 and 12,969 eddy trajectories respectively (with lifetimes larger than 4 weeks). Overall, eddies from upwelling networks account for only 10% of the total number of trajectories tracked in the Atlantic by the TOEddies algorithm. However, if we only consider long-lived eddies from these networks (with lifetimes greater than 52 weeks), this percentage increases to 61%. Mesoscale eddies of order zero (originating from the upwelling areas) were mostly cyclonic, accounting for 75% of the order-zero eddy trajectories for the BCUS and 57% for the CCUS (lifetimes ≥ 16 weeks). Nevertheless, anticyclonic eddies were also involved in the advection of properties when higher orders of interactions are considered. Indeed, the role of anticyclonic eddies on the advection and entrainment of upwelled waters when situated near upwelling coastal areas has been previously highlighted for both the CCUS and the BCUS (Duncombe Rae et al., 1992; Arístegui et al., 1997). When merging and splitting events are taken into account, both eddy types ensured connections between the eastern and western boundaries contributing to a mean connectivity signal (**Figure 9**).

The EBUS eddy-network reconstruction shows that long-lived and long-propagating eddies, along with their frequent interactions, may potentially transport waters from the upwelling regions further offshore and in some cases even reach the western Atlantic boundaries (Guerra et al., 2018; Nencioli et al., 2018; Laxenaire et al., 2018; Laxenaire et al., 2019) In order to investigate whether these connections concern only upper-ocean dynamics, we selected all Argo floats co-localised with the TOEddies Atlas that were identified inside the BCUS and CCUS network trajectories (**Figure 9**). Together, BCUS and CCUS eddy networks were sampled by 28,554 Argo profiles in various positions inside eddies. Around 21% of the total EBUS network trajectories were sampled by at least 1 Argo float. Out of these, 64% sampled anticyclones and 36% cyclones.

In order to estimate the mean connectivity signal represented by these mesoscale eddies in comparison with the adjacent environment, in **Figure 10** we plotted mean anomalies of potential temperature estimated from the CCUS and BCUS eddy networks in the upper ($\langle \gamma^n \rangle$ = 25 - 26 kg m^{-3}) and thermocline ($\langle \gamma^n \rangle$ = 26 - 27 kg m^{-3}) isopycnal layers. Anomalies were computed by subtracting the non-eddy climatology in each isopycnal surface. Positive and negative temperature anomalies corresponded to anticyclonic and cyclonic eddies respectively. These properties concerned only Argo floats trapped inside eddy trajectories with origins from the eastern upwelling system (we limited the estimate to up to order 5 trajectories in **Figure 9**). The subsurface extent of eddy properties was visible well below the surface, reaching intermediate depths.

On average, for the CCUS network, anticyclones were associated with mean temperature/salinity anomalies of about 0.45 ± 0.91°C/0.02 ± 0.14 g/kg in the upper layers and 0.26 ± 0.47°C/0.04 ± 0.09 g/kg for denser layers. For the BCUS, these mean temperature/salinity anomalies were stronger for both, the upper layers (0.93 ± 1.29°C/0.1 ± 0.18 g/kg) and for denser layers

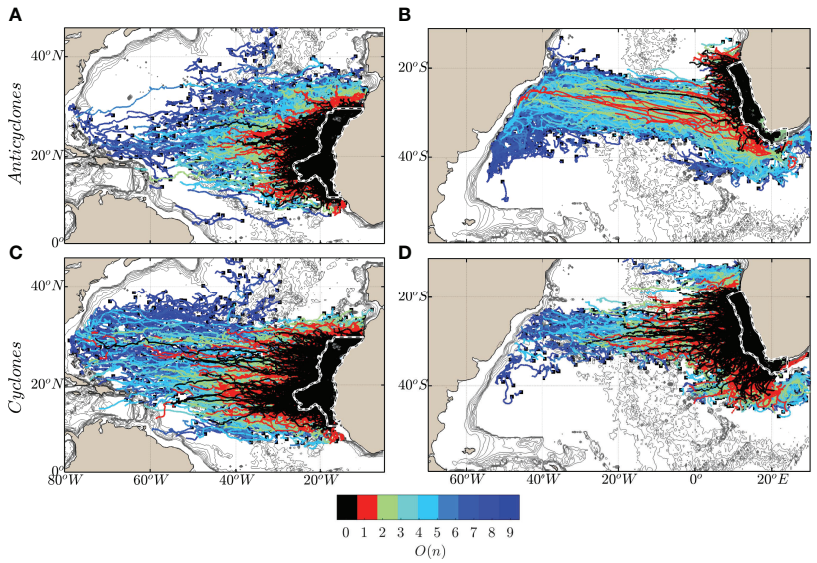

FIGURE 9 | Eddy network of anticyclonic **(A, B)** and cyclonic **(C, D)** trajectories from the CCUS (left panels) and the BCUS (right panels). Each eddy trajectory is colored according to their assigned order. Bathymetry shallower than 4,000 m is indicated by gray lines.

(0.95 ± 0.94°C/0.12 ± 0.12 g/kg). For CCUS cyclonic eddies, the mean temperature/salinity anomalies were estimated at -0.4 ± 1°C/-0.004 ± 0.12 g/kg for the upper layers and slightly weaker at greater depth (-0.39 ± 0.6°C/-0.04 ± 0.1 g/kg). Finally, BCUS anomalies for cyclones were found to be even positive in the upper isopycnal layers 0.08 ± 1°C/-0.04 ± 0.15 g/kg but reached -0.67± 0.9°C/-0.08 ± 0.11 g/kg for deeper layers.

The mean properties from the eddy networks demonstrated an additional contribution and spreading of heat and salt by mesoscale eddies in comparison with the environment. The comparison between upper and deeper isopycnal layer anomalies indicated that cross-basin connectivity achieved by mesoscale eddies not only concerns the upper layers but seems to extend down to the main thermocline. For BCUS cyclones the maximum of intense anomalies was found to be even stronger in the denser layers here considered ($\langle\gamma^n\rangle$ = 26 - 27 kg m^{-3}) than in the upper layers.

3.4 Individual Eddy Trajectories

In the previous section, by combining available hydrographic properties from Argo floats with the eddy trajectory networks built for the CCUS and BCUS, we estimated the mean temperature and salinity anomalies within isopycnal layers related to mesoscale eddies of EBUS origins in the Atlantic. These mean anomalies of properties associated with eddies are not restricted in the surface layers but can extend through the thermocline. In order to further evaluate vertical eddy properties and how they evolve over time we searched for individual eddy trajectories that were sufficiently sampled by Argo floats among the years of observations.

From the total eddy trajectories networks, we therefore selected specific examples of cyclonic and anticyclonic trajectories that were sampled by more than 30 Argos floats over periods of more than one year, allowing us to gather information on their internal structure along their en-route propagation. Among these, we firstly identified several Agulhas Rings that were previously described in Laxenaire et al. (2019, 2020) and for this reason, omit their discussion in this paper. We further isolated two specific cases of cyclonic eddies in the years 2012 and 2015 that were sampled by a total of 41 and 44 Argo profiles, the dynamical evolution of which we will describe in the following section. To our knowledge, these are among the few occurrences of Argo floats remaining trapped inside coherent cyclones for significant long time periods, providing us with information on their vertical structure and evolution.

3.4.1 BCUS Cyclones: Eddy Signature on Subduction

Figure 11 A shows the trajectories of two cyclonic eddies, C0 and C1, one originating from the nBCUS and one from the sBCUS and sampled by more than 30 profiles (magenta points) during their lifespans. These two cyclones were formed in late fall, in March 2012 (C1) and April 2015 (C0) respectively. They moved mainly west-southwestward and were tracked for more than 1 year with TOEddies. The movies of the two cyclones' dynamical evolution (see Supporting Information) show their daily tracking by TOEddies in the sea surface height fields along with their sampling rate from the Argo floats.

Several snapshots along the temporal evolution of the surface signature of these eddies are presented in **Figure 12**. Cyclone C0 was initially detected on 5 January 2015 in the nBCUS upwelling frontal zone and was tracked with TOEddies till 1 April 2016, for almost 65 weeks (approximately 1.5 years). The eddy drifted westward covering a distance of 1,793 km, while an Argo float (WMO 1901310) sampled C0 at various radial distances from the eddy center providing in total 44 T/S profiles. According to the

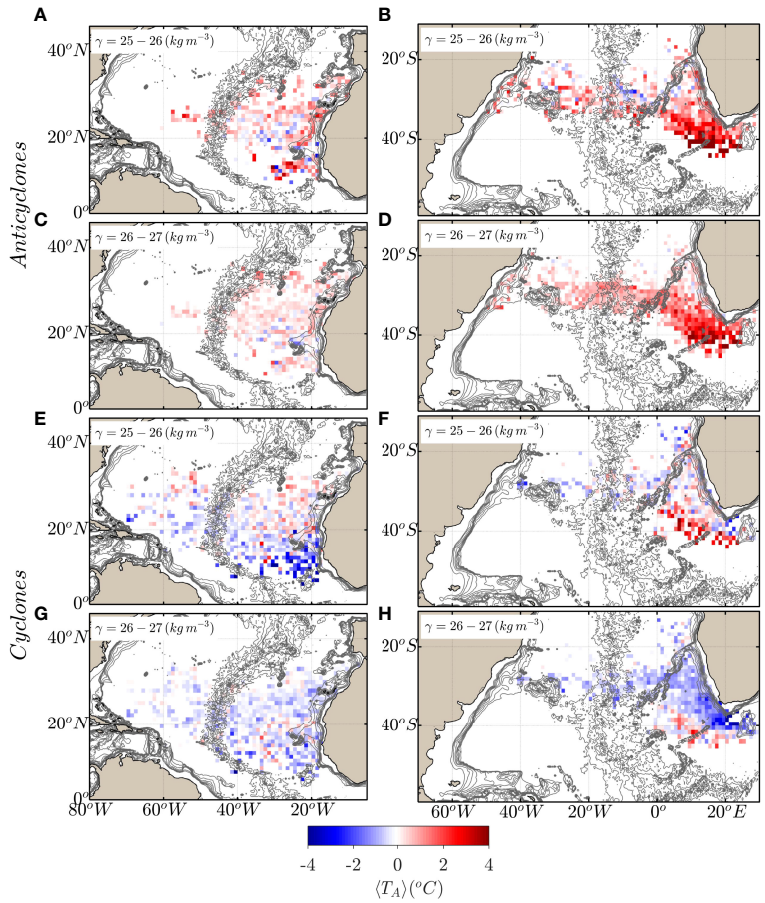

FIGURE 10 | Mean temperature anomalies $\langle T_A \rangle$ (°C) at upper (γ = 25 - 26 kg m^{-3}) **(A, B, E, F)** and deeper (γ = 26 - 27 kg m^{-3}) **(C, D, G, H)** isopycnal layers as measured by Argo floats trapped inside anticyclones and cyclones from the CCUS (left panels) and the BCUS (right panels) eddy trajectory networks. Bathymetry shallower than 4,000 m is indicated by gray lines.

TOEddies network reconstruction, this cyclone merged on 25 Feb 2015 with a short-lived cyclone (less than one month old) initially detected on 18 January 2015 (**Figure 12A**). It also seems that this eddy detached from the nBCUS slightly south of C0 (11.39°E, 26.55°S), and was sampled by the same Argo float that later remained trapped in C0 for almost 8 months. During eddy generation, while eddy scales and the distance from the shore remain relatively small, we cannot guarantee that satellite altimetry resolution is sufficiently accurate to resolve such rapid interactions between eddies. Nevertheless, this detachment was identified as a merging event by TOEddies. The Argo T/S profiles before and after the merging event showed that the eddy water masses were not significantly impacted. During the months that followed, the eddy propagated westward reaching and crossing the Walvis Ridge during the austral winter (June, July, August) of 2015 (**Figures 12C, D**).

Meanwhile, cyclone C1 was initially detected in sBCUS on 27 February 2012, north-west of Cape Town. This cyclone was tracked with TOEddies for almost 71 weeks (16 months). From March 2012 several different Argo floats sampled the eddy until 12 July 2013 when the eddy was last detected, providing 41 vertical profiles. From August 2012, the cyclone drifted westward while starting to interact with and propagate along an Agulhas Ring that was in the vicinity (**Figures 12G–H**). Such cyclone-anticyclone interactions in the Cape Basin have been previously documented from observations (Boebel et al., 2003; Souza et al., 2011) and numerical simulations (Doglioli et al., 2007).

Figures 11B, C depict the daily evolution of the geostrophic dynamical characteristics of the radii and azimuthal velocities of the two eddies under investigation. The time series for C1 and C0 show distinct dynamical periods for the eddies. During generation, when the eddies were moving away from the continental slope, variations in their velocity and radius were observed. After generation both cyclones increased in radius and velocity. The latter thus reached a maximum of 40 cm/s and 60 cm/s for cyclones C0 and C1 respectively, 6 months after generation (**Figure 11C**). It is worth noting that the maximum eddy intensities are at least twice as high as than the mean CE intensities shown in Section 3.2. Indeed, for C0, during the austral summer, the eddy diameter remained constant whereas the eddy tangential speed increased when the eddy crossed the Walvis Ridge. During that period, its translation speed was

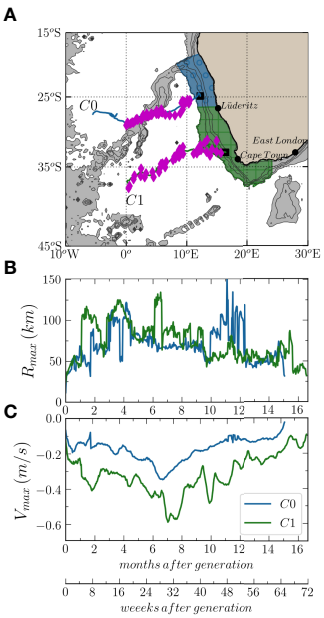

FIGURE 11 | Trajectories of long-lived cyclones C0 and C1 originating from the sBCUS (green patch) and nBCUS (blue patch) as detected from the TOEddies database for the years 2012 and 2015 respectively are shown in **A**. Bathymetry shallower than 4,000 m is indicated by gray shading. The temporal evolution of dynamical characteristics of characteristic radius R_{max} (km) and velocity V_{max} (m/s) is shown in **B**, **C**.

relatively weak (~ 7 km/day), and its shape remained almost circular with ellipticity below $\epsilon = 0.3$. A decay in the eddy velocity was then observed.

In order to investigate the evolution of the vertical structure of the eddies core, we selected only Argo profiles that were located at a radial distance of ≤ 55 km from their estimated centers (**Figures 13A, B**). This corresponds to a mean ratio between the Argo radial distance and the eddy characteristic radius of about 50% (maximum ratio of about 74%). The temporal evolution of the temperature and density anomalies in the cores of the two cyclones is shown in **Figures 13C, D** along with the estimation of their mixed layer depth (MLD). The latter was determined by computing the depth at which the Brunt–Väisälä frequency squared ($N^2 = -\frac{g}{f}\frac{\partial \rho}{\partial z}$) was found to be at its minimum. We then estimated the density anomaly induced by the eddies on the basis of the climatological eddy background containing a no-eddy signature (**Figures 13E, F**). To quantify the vertical extent of the eddy we computed the depth of the maximal density anomaly.

According to **Figure 13** during the first 3 months of the formation of C0, the density anomaly of the eddy seemed weak in comparison with the surrounding environment. This makes sense when considering that the eddy had not yet detached from the shelf and the upwelling tongue: during this period the eddy was mainly trapped in the upwelled waters that were not significantly different from the adjacent environment. Once the eddy started to propagate westward, we then detected a temperature and salinity anomaly located

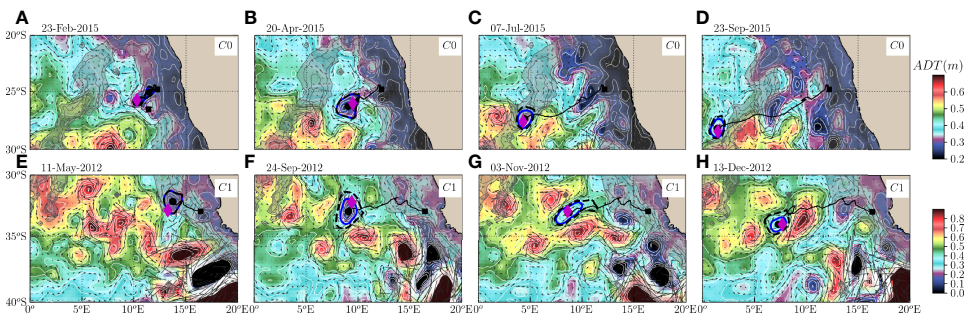

FIGURE 12 | Snapshots along the temporal evolution of cyclones C0 **(A–D)** and C1 **(E–H)**. The background colors correspond to the ADT while the gray arrows correspond to surface geostrophic velocities. The characteristic and outer contours detected by TOEddies are shown by the solid blue and dashed black lines. The Argo floats trapped in the eddies are shown by magenta diamonds points. Bathymetry shallower than 4,000 m is indicated by gray shading.

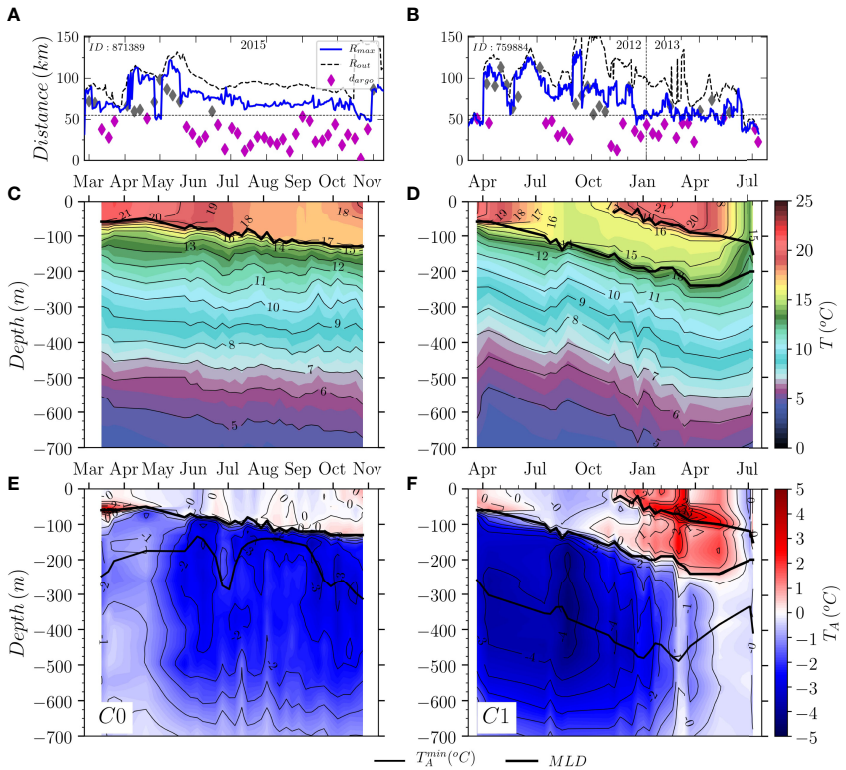

FIGURE 13 | The temporal evolution of eddy characteristic R_{max} (km) and outermost radius R_{out} (km) is shown in panels **(A, B)**, with the blue and black dashed lines indicating cyclones C0 and C1 respectively. The magenta diamond points illustrate the position of the Argo profiles as a function of their distance from the eddy center. Vertical profiles of temperature T (°C)as obtained from the Argo floats trapped in the eddy are shown in panels **(C, D)**. The vertical temperature T_A (°C) anomalies are shown in panels **(E, F)** relative to the TOEddies climatology.

at between -200 and -700 m depth, which was -2.8°C/-0.3 g/kg colder and fresher than the environment. The density anomaly of C0 was confined to between -100 and -700 m depth with a maximal density anomaly of σ_A = 0.34 kg m^{-3} that was located at -190 m in May 2015. Two months later, the maximal density anomaly seemed to deepen further, reaching Z_{max} = -210 m on 30 July 2015. In September 2015, the maximal density anomaly reached a depth of Z_{max} = -240 m while remaining relatively strong σ_A = 0.37 kg m^{-3} (with -3.4°C/-0.37 g/kg temperature and salinity anomalies). Unfortunately, no other Argo float was detected inside the eddy after November 2015 despite TOEddies managing to track it until 1 April 2016 (5.5°W, 27.54°S).

As for C1, one month after its formation (on 22 March 2012), the eddy density anomaly was σ_A = 0.52 kg m^{-3} at -80 m. Five months later, the maximal σ_A remained the same in intensity while deepening, reaching a depth of Z_{max} = -180 m on 25 August 2012, with corresponding temperature and salinity anomalies of -4.4°C/-0.47 g/kg. In November 2012, the maximal density anomaly deepened further reaching Z_{max} = -250 m probably as a result of air-sea interactions that cooled and mixed the eddy upper layers, deepening its MLD. Indeed, during that period the eddy's upper layers seemed to be connected to the surface. From November till at least March 2013 (austral summer), in the upper eddy structure, a seasonal thermocline appeared, whereas the eddy core seemed to penetrate further in depth while gradually separating from the ocean surface. Afterwards, the eddy propagated south-westward (0.57°E, 37.9°S) until 12 July 2013 when it was last detected.

The vertical sampling of the two BCUS cyclones, C0 and C1, shows that these eddies accounted for density anomalies of σ_A = 0.5 kg m^{-3} and temperature anomalies of 4.4°C in the Cape Basin. Both cyclonic eddies showed a progressive deepening of their vertical structure and a clear separation from the ocean surface, suggesting that they subsided and became subsurface-intensified eddies as they left the upwelling area and penetrated the Cape Basin. This transition was accompanied by a gradual decay of both eddy surface intensities whereas subsurface anomalies remained relatively unchanged.

Such behavior has been already observed and described for anticyclonic eddies, in particular for Agulhas Rings and for CCUS specific anticyclones (Schütte et al., 2016a; Karstensen et al., 2017; Barceló-Llull et al., 2017; Guerra et al., 2018; Laxenaire et al., 2019; Laxenaire et al., 2020). (Laxenaire et al., 2019; Laxenaire et al., 2020) showed that the majority of Agulhas Rings become subsurface-intensified eddies along their route. However, the results we discuss

in the present study, represent the first evidence of such behavior for cyclonic eddies in the South Atlantic.

4 SUMMARY AND CONCLUSION

Motivated by the fact that EBUS are areas of high productivity as well as of frequent eddy generation, we examined cross-basin oceanic connectivity that is promoted by coherent, long-lived and long-propagating mesoscale eddies with eastern upwelling origins in the Atlantic Ocean. We characterized the dynamical properties of mesoscale eddies over a 24-year period (1993 to 2018) throughout the Atlantic with the TOEddies Dynamical Dataset that uses daily satellite observations of ADT.

Among all the mesoscale eddies detected in the Atlantic Ocean with the TOEddies dataset, a small fraction of them will be long-lived (10% with lifetimes more than 52 weeks). In agreement with previous studies (Chaigneau et al., 2009; Chelton et al., 2011), we found that long-lived eddies propagate mainly westward and are predominantly anticyclonic. However, at least 60% of these long-lived westward eddies were found to either originate or interact with eddies from eastern boundary upwelling systems. We have then specifically qualified from the whole Atlantic TOEddies dataset the eddies spawn from the four upwelling subsystems (north and south CCUS and BCUS), analyzing their seasonal and interannual variabilities. By using co-localized Argo float profiles, also provided by the TOEddies Atlantic Atlas, we characterized their mean vertical structures, retaining only the Argo profiles sampling the eddies' dynamical cores.

To estimate the contribution of eddies on oceanic connectivity, we reconstructed the eddy-trajectory network linking eddies of upwelled origins to all nearby eddies connected to them *via* merging/and splitting events. The mean eddy connectivity signal was then derived on the basis of a synthesis of the CCUS and BCUS eddy networks with 17 years of *in-situ* observations from Argo floats. A comparison between eddies from the four upwelling subsystems showed that a higher number of eddy trajectories is associated with cyclonic than anticyclonic eddies. The only exception to this observation is the nCCUS subsystem characterized by an equal proportion of eddies of each polarity. In total numbers, more eddies were detected to originate from the CCUS than the BCUS. On the other hand, our study suggests that the sBCUS is mainly characterized by cyclonic eddies (83%), the mean tangential velocity of which is about double the intensity of cyclones from the other subsystems. Our comparisons with mean upwelling indicators as derived from ERA5 datasets showed that seasonal variations in eddy formation do not always coincide with the mean upwelling climatology. Further investigation of possible connections between specific eddy formations and the processes responsible for their variability is therefore required (Marchesiello et al., 2003; Marchesiello and Estrade, 2007; Moscoso et al., 2021).

We retracted the Canary eddy corridor, first introduced in Sangrà et al. (2009), for the CCUS, while also tracking long-lived eddies that propagated even farther than 35°W. Similar eddy westward pathways were found for the BCUS. Poleward/equatorward deflections for cyclonic/anticyclonic eddies were also confirmed in our study. Nevertheless, cyclones originating from the sCCUS and nBCUS were found to propagate mostly westward, also joining the southern branch of the South Equatorial Current (Majumder et al., 2019; Luko et al., 2021). Several of the upwelled-origin eddies that we investigated, contributed to a mean oceanic connectivity across basins, for example when they managed to reach the western boundary current systems. Eddy mean lifetimes may exceed 1 year and propagation distances of 2,000 km. Moreover, we noted that these eddies were not isolated but often merged and splitted with other structures. We expect that during such events, the resulting eddies will remain stable and retain some fraction of the initial trapped waters. Besides, coherent eddies may interact and exchange properties *via* their mutual deformation (Dritschel, 1995; Yasuda, 1995; Yasuda and Flierl, 1995; Carton, 2001; Flament et al., 2001; Brandt and Nomura, 2010; Carton et al., 2015). When taking into account eddy-eddy interactions, both cyclonic and anticyclonic eddies are important in transporting water properties across-basins. The mean thermohaline structure as derived from the combination of eddy trajectories with available Argo float measurements displays a mean connectivity signal between eastern and western boundaries that does not only concern surface layers but may extend deeper. On average the vertical extent of eddies from the CCUS was found to be shallower (maximum temperature anomalies ranging between 50 - 190 m, γ^n = 25.2 - 27.1 kg m^{-3}) than that of eddies from the BCUS which occupyied deeper and denser layers (150 - 530 m, γ^n = 26.5 - 27.14 kg m^{-3}). Mean anomalies associated with BCUS cyclonic eddies were found to be even stronger along the lower thermocline isopycnal layers (γ^n = 26.5 - 27 kg m^{-3}).

Finally, we focused on two specific years in which two cyclonic eddies originating from the nBCUS and sBCUS were formed. During these years, Argo profilers were trapped for several months in their cores, allowing us to compare the temporal evolution of their hydrological properties. The two cyclonic eddies that were sampled by Argo floats along their en-route propagation provided additional observational evidence of the transport of properties by coherent eddies. The temporal evolution of their anomalies revealed a progressive deepening of the eddy core into deeper thermocline layers while being advected further west, suggesting a subduction and a transformation of these eddies from surface-intensified to subsurface-intensified structures. Cyclone C0 originating from the nBCUS crossed the Walvis Ridge and left the Cape Basin, contrary to previous findings (Matano and Beier, 2003). Moreover, the multi-month vertical sampling of this eddy by Argo floats showed that the eddy's core remained unchanged while crossing the Walvis Ridge. While the subduction process has previously been evidenced for Agulhas Rings (Laxenaire et al., 2019; Laxenaire et al., 2020), to our knowledge, this study represents the first description of subduction for cyclonic eddies. Indeed, subsurface eddies have already been surveyed in similar EBUS areas, for example in the CCUS (Schütte et al., 2016a,b; Karstensen et al., 2017; Dilmahamod et al., 2021).

We note that our study provides information for only a small fraction of eddies whose signature is detectable from altimetry maps. With the current satellite and *in-situ* observations and the TOEddies algorithm, we can only observe part of all mesoscale eddy processes that occur in the ocean, and even these provide only partial glimpses of these events. We hope that with the upcoming altimetry SWOT mission together with dedicated field experiments, it will be possible to gain new insight. The SWOT wide-swath altimetric signal is expected to capture, with higher accuracy, ocean-surface topography globally but also near the BCUS area. Nevertheless, our results already suggest that the Atlantic eastern boundary upwelling systems are important sources of long-lived eddies that may efficiently export heat, salt and other water properties further offshore from the coastal upwelling areas. As documented in this study for two cyclonic eddies spawn from the BCUS, or Agulhas Rings (Laxenaire et al., 2019, Laxenaire et al., 2020) or anticyclones in the CCUS (Schütte et al., 2016a, b; Karstensen et al., 2017; Dilmahamod et al., 2021), many eddies subduct into the subsurface while drifting westward. We therefore suggest that most of the eddies that disappear from altimetry maps do not immediately dissipate but continue to drift into the open ocean, masked by upper-ocean layer stratification. Their potential impact on thermocline ventilation and coastal ecosystems should be addressed in future studies. Indeed, these eddies trap and advect water properties as well as plankton and fish larvae from the nutrient-rich upwelling shelfs. Their ability to connect distant environments should thus be investigated further.

DATA AVAILABILITY STATEMENT

The data used for this paper are available at the following repository and can be accessed through the following link (10.5281/zenodo.6443096). The gridded satellite altimetry data we used in this work were produced by SSALTO/DUACS and distributed by the Copernicus Marine Environment Monitoring Service (https://marine.copernicus.eu/). The Argo data were collected and made freely available by the International Argo Program and the national programs that contribute to it (https://coriolis.eu.org).

AUTHOR CONTRIBUTIONS

AI and SS designed the study and contributed to the writing. AI performed the data analysis while RL provided TOEddies dataset and automatic eddy detection for the study area. All authors contributed to the article and approved the submitted version.

FUNDING

This paper was supported by the TRIATLAS project, which has received funding from the European Union's Horizon 2020 research and innovation programme under grant agreement No 817578.

ACKNOWLEDGMENTS

We would like to gratefully acknowledge and thank the two reviewers for their comments that helped us improve the manuscript and Johannes Karstensen from the GEOMAR Helmholtz Centre for Ocean Research in Kiel for his helpful suggestions and bibliographic input. This work was supported by the European Union's Horizon 2020 research and innovation program under grant agreements no. 817578 (TRIATLAS), the TOEddies and BIOSWOT CApeCauldron CNES-TOSCA and the ENS Chaire Chanel research grants. We also acknowledge the mesoscale calculation server CICLAD (http://ciclad-web.ipsl.jussieu.fr) dedicated to Institut Pierre Simon Laplace modeling effort for technical and computational support.

SUPPLEMENTARY MATERIAL

The Supplementary Material for this article can be found online at: https://www.frontiersin.org/articles/10.3389/fmars.2022.835260/full#supplementary-material

REFERENCES

Amores, A., Jordà, G., Arsouze, T., and Le Sommer, J. (2018). Up to What Extent Can We Characterize Ocean Eddies Using Present-Day Gridded Altimetric Products? *J. Geophys. Res.: Oceans* 123, 7220–7236. doi: 10.1029/2018JC014140

Amos, C. M., Castelao, R. M., and Medeiros, P. M. (2019). Offshore Transport of Particulate Organic Carbon in the California Current System by Mesoscale Eddies. *Nat. Commun.* 10, 1–21. doi: 10.1038/s41467-019-12783-5

Arhan, M., Mercier, H., and Lutjeharms, J. R. E. (1999). The Disparate Evolution of Three Agulhas Rings in the South Atlantic Ocean. *J. Geophys. Res.: Oceans* 104, 20987–21005. doi: 10.1029/1998JC900047

Arhan, M., Speich, S., Messager, C., Dencausse, G., Fine, R., and Boye, M. (2011). Anticyclonic and Cyclonic Eddies of Subtropical Origin in the Subantarctic Zone South of Africa. *J. Geophys. Res.: Oceans* 116, 1–22. doi: 10.1029/2011JC007140

Arístegui, J., and Montero, M. F. (2005). Temporal and Spatial Changes in Plankton Respiration and Biomass in the Canary Islands Region: The Effect of Mesoscale Variability. *J. Mar. Syst.* 54, 65–82. doi: 10.1016/j.jmarsys.2004.07.004

Arístegui, J., Sangrá, P., Hernández-León, S., Cantón, M., Hernández-Guerra, A., and Kerling, J. (1994). Island-Induced Eddies Canary Islands. *Deep-Sea Res.* 41, 1509–1525. doi: 10.1016/0967-0637(94)90058-2

Arístegui, J., Tett, P., Hernández-Guerra, A., Basterretxea, G., Montero, M., Wild, K., et al. (1997). The Influence of Island-Generated Eddies on Chlorophyll Distribution: A Study of Mesoscale Variation Around Gran Canaria. *Deep-Sea Res. I* 44, 71–96. doi: 10.1016/s0967-0637(96)00093-3

Assassi, C., Morel, Y., Vandermeirsch, F., Chaigneau, A., Pegliasco, C., and Morrow, R. (2016). An Index to Distinguish Surface- and Subsurface-Intensified Vortices From Surface Observations. *J. Phys. Oceanography* 46, 2529–2552. doi: 10.1175/JPO-D-15-0122.1

Barceló-Llull, B., Sangrà, P., Pallàs-Sanz, E., Barton, E. D., Estrada-Allis, S. N., Martínez-Marrero, A., et al. (2017). Anatomy of a Subtropical Intrathermocline Eddy. *Deep Sea Res. Part I: Oceanogr. Res. Papers* 124, 126–139. doi: 10.1016/j.dsr.2017.03.012

Barton, E., Arístegui, J., Tett, P., Cantón, M., García-Braun, J., Hernández-León, S., et al. (1998). The Transition Zone of the Canary Current Upwelling Region. *Prog. Oceanography* 41, 455–504. doi: 10.1016/S0079-6611(98)00023-8

Barton, E. D., Arístegui, J., Tett, P., and Pérez, E. N. (2004). Variability in the Canary Islands Area of Filament-Eddy Exchanges. *Prog. Oceanography* 62, 71–94. doi: 10.1016/j.pocean.2004.07.003

Basterretxea, G., Barton, E., Tett, P., Sangrá, P., Navarro-Perez, E., and Arístegui, J. (2002). Eddy and Deep Chlorophyl Maximum Response to Wind-Shear in the Lee of Gran Canaria. *Deep-Sea Res. I* 49, 1087–1101. doi: 10.1016/S0967-0637(02)00009-2

Benazzouz, A., Mordane, S., Orbi, A., Chagdali, M., Hilmi, K., Atillah, A., et al. (2014). An Improved Coastal Upwelling Index From Sea Surface Temperature Using Satellite-Based Approach – The Case of the Canary Current Upwelling System. *Cont. Shelf Res.* 81, 38–54. doi: 10.1016/j.csr.2014.03.012

Blamey, L. K., Shannon, L. ., Bolton, J. J., Crawford, R. J., Dufois, F., Evers-King, H., et al. (2015). Ecosystem Change in the Southern Benguela and the Underlying Processes. *J. Mar. Syst.* 144, 9–29. doi: 10.1016/j.jmarsys.2014.11.006

Blanke, B., Penven, P., Roy, C., Chang, N., and Kokoszka, F. (2009). Ocean Variability Over the Agulhas Bank and its Dynamical Connection With the Southern Benguela Upwelling System. *J. Geophys. Res.* 114, 1–15. doi: 10.1029/2009JC005358

Boebel, O., Lutjeharms, J., Schmid, C., Zenk, W., Rossby, T., and Barron, C. (2003). The Cape Cauldron: A Regime of Turbulent Inter-Ocean Exchange. Deep Sea Research Part II: Topical Studies in Oceanography. *Earth System Science Data* 50, 57–86. doi: 10.1016/s0967-0645(02)00379-x

Brandt, P., Bange, H. W, Banyte, D., Dengler, M., Didwischus, S.-H., and Fischer, T. (2015). On the Role of Circulation and Mixing in the Ventilation of Oxygen Minimum Zones With a Focus on the Eastern Tropical North Atlantic. *Biogeosciences* 12, 489–512. doi: 10.5194/bg-12-489-2015

Brandt, L. K., and Nomura, K. K. (2010). Characterization of the Interactions of Two Unequal Co-Rotating Vortices. *J. Fluid Mech.* 646, 233–253. doi: 10.1017/s0022112009992849

Caldeira, R. M. A., Stegner, A., Couvelard, X., Araújo, I. B., Testor, P., and Lorenzo, A. (2014). Evolution of an Oceanic Anticyclone in the Lee of Madeira Island: *In Situ* and Remote Sensing Survey. *J. Geophys. Res.: Oceans* 119, 1195–1216. doi: 10.13140/2.1.4081.7926

Carton, X. (2001). Hydrodynamical Modeling Of Oceanic Vortices. *Surveys Geophys.* 22, 179–263. doi: 10.1023/a:1013779219578

Carton, X., Ciani, D., Verron, J., Reinaud, J., and Sokolovskiy, M. (2015). Vortex Merger in Surface Quasi-Geostrophy. *Geophys. Astrophys. Fluid Dynamics* 110, 1–22. doi: 10.1080/03091929.2015.1120865

Chaigneau, A., Eldin, G., and Dewitte, B. (2009). Eddy Activity in the Four Major Upwelling Systems From Satellite Altimetr–2007). *Prog. Oceanography* 83, 117–123. doi: 10.1016/j.pocean.2009.07.012

Chaigneau, A., Le Texier, M., Eldin, G., Grados, C., and Pizarro, O. (2011). Vertical Structure of Mesoscale Eddies in the Eastern South Pacific Ocean: A Composite Analysis From Altimetry and Argo Profiling Floats. *J. Geophys. Res.: Oceans* 116, 1–16. doi: 10.1029/2011JC007134

Chelton, D. B, Schlax, M. G., and Samelson, R. M. (2011). Global Observations of Nonlinear Mesoscale Eddies. *Prog. Oceanography* 91, 167–216. doi: 10.1016/j.pocean.2011.01.002

Cornec, M., Claustre, H., Mignot, A., Guidi, L., Lacour, L., Poteau, A., et al. (2021a). Deep Chlorophyll Maxima in the Global Ocean: Occurrences, Drivers and Characteristics. *Global Biogeochem. Cycles* 35, e2020GB006759. doi: 10.1029/2020gb006759

Cornec, M., Laxenaire, R., Speich, S., and Claustre, H. (2021b). Impact of Mesoscale Eddies on Deep Chlorophyll Maxima. *Geophys. Res. Lett.* 48, e2021GL093470. doi: 10.1029/2021gl093470

Correa-Ramirez, M. A., Hormazábal, S., and Yuras, G. (2007). Mesoscale Eddies and High Chlorophyll Concentrations Off Central Chile (29°–39°s). *Geophys. Res. Lett.* 34, 1–5. doi: 10.1029/2007GL029541

Cui, W., Wang, W., Zhang, J., and Yang, J. (2019). Multicore Structures and the Splitting and Merging of Eddies in Global Oceans From Satellite Altimeter Data. *Ocean Sci.* 15, 413–430. doi: 10.5194/os-15-413-2019

Cury, P., and Shannon, L. (2004). Regime Shifts in Upwelling Ecosystems: Observed Changes and Possible Mechanisms in the Northern and Southern Benguela. *Prog. Oceanography* 60, 223–243. doi: 10.1016/j.pocean.2004.02.007

de Marez, C., L'Hégaret, P., Morvan, M., and Carton, X. (2019). On the 3D Structure of Eddies in the Arabian Sea. *Deep Sea Res. Part I: Oceanogr. Res. Papers* 150, 103057. doi: 10.1016/j.dsr.2019.06.003

Desbiolles, F., Blanke, B., Bentamy, A., and Grima, N. (2014). Origin of Fine-Scale Wind Stress Curl Structures in the Benguela and Canary Upwelling Systems. *J. Geophys. Res.: Oceans* 119, 7931–7948. doi: 10.1002/2014JC010015

Dilmahamod, A. F., Aguiar-González, B., Penven, P., Reason, C. J. C., Ruijter, W. P. M. D., Malan, N., et al. (2018). SIDDIES Corridor: A Major East-West Pathway of Long-Lived Surface and Subsurface Eddies Crossing the Subtropical South Indian Ocean. *J. Geophys. Res.: Oceans* 123, 5406–5425. doi: 10.1029/2018jc013828

Dilmahamod, A. F, Karstensen, J., Dietze, H., Löptien, U., and Fennel, K. (2021). Generation Mechanisms of Mesoscale Eddies in the Mauritanian Upwelling Region. *J. Phys. Oceanography* 52(1), 161–182. doi: 10.1175/jpo-d-21-0092.1

Doglioli, A., Blanke, B., Speich, S., and Lapeyre, G. (2007). Tracking Coherent Structures in a Regional Ocean Model With Wavelet Analysis: Application to Cape Basin Eddies. *J. Geophys. Res.* 112, 1–12. doi: 10.1029/2006jc003952

Dritschel, D. G. (1995). A General Theory for Two-Dimensional Vortex Interactions. *J. Fluid Mech.* 293, 269–303. doi: 10.1017/s0022112095001716

Dufois, F., Hardman-Mountford, N. J, Greenwood, J., Richardson, A. J, Feng, M., and Matear, R. J. (2016). Anticyclonic Eddies are More Productive Than Cyclonic Eddies in Subtropical Gyres Because of Winter Mixing. *Sci. Adv.* 2, e1600282. doi: 10.1126/sciadv.1600282

Duncombe Rae, C., Shillington, F., Agenbag, J., Taunton-Clark, J., and Gründlingh, M. (1992). An Agulhas Ring in the South Atlantic Ocean and its Interaction With the Benguela Upwelling Frontal System. Deep Sea Research Part A. *Oceanogr. Res. Papers* 39, 2009–2027. doi: 10.1016/0198-0149(92)90011-H

Du, Y., Yi, J., Wu, D., He, Z., Wang, D., and Fuyuan, L. (2014). Mesoscale Oceanic Eddies in the South China Sea From 1992 to 2012: Evolution Processes and Statistical Analysis. *Acta Oceanol. Sin.* 33, 36–47. doi: 10.1007/s13131-014-0530-6

Flament, P., Lumpkin, R., Tournadre, J., and Armi, L. (2001). Vortex Pairing in an Unstable Anticyclonic Shear Flow: Discrete Subharmonics of One Pendulum Day. *J. Fluid Mech.* 440, 401–409. doi: 10.1017/s0022112001004955

Flierl, G. R. (1981). Particle Motions in Large-Amplitude Wave Fields. *Geophys. Astrophys. Fluid Dynamics* 18, 39–74. doi: 10.1080/03091928108208773

Giulivi, C. F, and Gordon, A. L. (2006). Isopycnal Displacements Within the Cape Basin Thermocline as Revealed by the Hydrographic Data Archive. *Deep Sea Res. Part I: Oceanogr. Res. Papers* 53, 1285–1300. doi: 10.1016/j.dsr.2006.05.011

Gruber, N., Lachkar, Z., Frenzel, H., Marchesiello, P., Münnich, M., McWilliams, J. C., et al. (2011). Eddy-Induced Reduction of Biological Production in Eastern Boundary Upwelling Systems. *Nat. Geosci.* 4, 787–792. doi: 10.1038/ngeo1273

Guerra, L. A. A., Paiva, A. M, and Chassignet, E. P. (2018). On the Translation of Agulhas Rings to the Western South Atlantic Ocean. *Deep Sea Res. Part I: Oceanogr. Res. Papers* 139, 104–113. doi: 10.1016/j.dsr.2018.08.005

Harvey, C. J., Fisher, J. L., Samhouri, J. F., Williams, G. D., Francis, T. B, Jacobson, K. C., et al. (2020). The Importance of Long-Term Ecological Time Series for Integrated Ecosystem Assessment and Ecosystem-Based Management. *Prog. Oceanography* 188, 102418. doi: 10.1016/j.pocean.2020.102418

Hersbach, H., Bell, B., Berrisford, P., Biavati, G., Horányi, A., Muñoz Sabater, J., et al. (2018). *ERA5 Hourly Data on Single Levels From 1979 to Present*. Copernicus Climate Change Service (C3S) Climate Data Store (CDS). doi: 10.24381/cds.adbb2d47

Hutchings, L., van der Lingen, C., Shannon, L., Crawford, R., Verheye, H., Bartholomae, C., et al. (2009). The Benguela Current: An Ecosystem of Four Components. *Prog. Oceanography* 83, 15–32. doi: 10.1016/j.pocean.2009.07.046

Ioannou, A., Stegner, A., Dubos, T., Le Vu, B., and Speich, S. (2020a). Generation and Intensification of Mesoscale Anticyclones by Orographic Wind Jets: The Case of Ierapetra Eddies Forced by the Etesians. *J. Geophys. Res.: Oceans* 125, e2019JC015810. doi: 10.1029/2019jc015810

Ioannou, A., Stegner, A., Dumas, F., and Vu, B. L. (2020b). Three-Dimensional Evolution of Mesoscale Anticyclones in the Lee of Crete. *Front. Mar. Sci.* 7. doi: 10.3389/fmars.2020.609156

Ioannou, A., Stegner, A., Le Vu, B., Taupier-Letage, I., and Speich, S. (2017). Dynamical Evolution of Intense Ierapetra Eddies on a 22 Year Long Period. *J. Geophys. Res.: Oceans* 122, 9276–9298. doi: 10.1002/2017jc013158

Karstensen, J., Schütte, F., Pietri, A., Krahmann, G., Fiedler, B., Grundle, D., et al. (2017). Upwelling and Isolation in Oxygen-Depleted Anticyclonic Modewater Eddies and Implications for Nitrate Cycling. *Biogeosciences* 14, 2167–2181. doi: 10.5194/bg-14-2167-2017

Kirkman, S., Blamey, L., Lamont, T., Field, J., Bianchi, G., Huggett, J., et al. (2016). Spatial Characterisation of the Benguela Ecosystem for Ecosystem-Based Management. *Afr. J. Mar. Sci.* 38, 7–22. doi: 10.2989/1814232X.2015.1125390

Laxenaire, R., Speich, S., Blanke, B., Chaigneau, A., Pegliasco, C., and Stegner, A. (2018). Anticyclonic Eddies Connecting the Western Boundaries of Indian and Atlantic Oceans. *J. Geophys. Res.: Oceans* 123, 7651–7677. doi: 10.1029/2018JC014270

Laxenaire, R., Speich, S., and Stegner, A. (2019). Evolution of the Thermohaline Structure of One Agulhas Ring Reconstructed From Satellite Altimetry and Argo Floats. *J. Geophys. Res.* 124, 8969–9003. doi: 10.1029/2018jc014426

Laxenaire, R., Speich, S., and Stegner, A. (2020). Agulhas Ring Heat Content and Transport in the South Atlantic Estimated by Combining Satellite Altimetry and Argo Profiling Floats Data. *J. Geophys. Res.: Oceans* 125, e2019JC015511. doi: 10.1029/2019jc015511

Lehahn, Y., d'Ovidio, F., Lévy, M., Amitai, Y., and Heifetz, E. (2011). Long Range Transport of a Quasi Isolated Chlorophyll Patch by an Agulhas Ring. *Geophys. Res. Lett.* 38, 1–6. doi: 10.1029/2011GL048588

Le Vu, B., Stegner, A., and Arsouze, T. (2018). Angular Momentum Eddy Detection and Tracking Algorithm (AMEDA) and Its Application to Coastal Eddy Formation. *J. Atmos. Oceanic Technol.* 35, 739–762. doi: 10.1175/jtech-d-17-0010.1

Li, Q.-Y., Sun, L., Liu, S.-S., Xian, T., and Yan, Y.-F. (2014). A New Mononuclear Eddy Identification Method With Simple Splitting Strategies. *Remote Sens. Lett.* 5, 65–72. doi: 10.1080/2150704X.2013.872814

Luko, C. D., Silveira, I. C. A., Simoes-Sousa, I. T., Araujo, J. M., and Tandon, A. (2021). Revisiting the Atlantic South Equatorial Current. *J. Geophys. Res.: Oceans* 126, e2021JC017387. doi: 10.1029/2021jc017387

Lumpkin, R. (2016). Global Characteristics of Coherent Vortices From Surface Drifter Trajectories. *J. Geophys. Res.: Oceans* 121, 1306–1321. doi: 10.1002/2015jc011435

Majumder, S., Goes, M., Polito, P. S, Lumpkin, R., Schmid, C., and Lopez, H. (2019). Propagating Modes of Variability and Their Impact on the Western Boundary Current in the South Atlantic. *J. Geophys. Res.: Oceans* 124, 3168–3185. doi: 10.1029/2018jc014812

Manta, G., Speich, S., Karstensen, J., Hummels, R., Kersalé, M., Laxenaire, R., et al. (2021). The South Atlantic Meridional Overturning Circulation and Mesoscale Eddies in the First GO-SHIP Section at 34.5°S. *J. Geophys. Res.: Oceans* 126, e2020JC016962. doi: 10.1029/2020JC016962

Marchesiello, P., and Estrade, P. (2007). Eddy Activity and Mixing in Upwelling Systems: A Comparative Study of Northwest Africa and California Regions. *Int. J. Earth Sci.* 98, 299–308. doi: 10.1007/s00531-007-0235-6

Marchesiello, P., McWilliams, J. C, and Shchepetkin, A. (2003). Equilibrium Structure and Dynamics of the California Current System. *J. Phys. Oceanography* 33, 753–783. doi: 10.1175/1520-0485(2003)33<753:esadot>2.0.co;2

Matano, R., and Beier, E. (2003). A Kinematic Analysis of the Indian/Atlantic Interocean Exchange. *Deep Sea Res. Part II: Topical Stud. Oceanography* 50, 229–249. doi: 10.1016/s0967-0645(02)00395-8

McDougall, T. J, and Barker, P. M. (2011). *Getting Started With TEOS-10 and the Gibbs Seawater (GSW) Oceanographic Toolbox*. Intergovernmental Oceanographic Commission IOC of Unesco

McGillicuddy, D. J., Anderson, L. A, Bates, N. R, Bibby, T., Buesseler, K. O, Carlson, C. A., et al. (2007). Eddy/Wind Interactions Stimulate Extraordinary Mid-Ocean Plankton Blooms. *Science* 316, 1021–1026. doi: 10.1126/science.1136256

Morrow, R. (2004). Divergent Pathways of Cyclonic and Anti-Cyclonic Ocean Eddies. *Geophys. Res. Lett.* 31, 1–5. doi: 10.1029/2004gl020974

Moscoso, J. E, Stewart, A. L, Bianchi, D., and McWilliams, J. C. (2021). The Meridionally Averaged Model of Eastern Boundary Upwelling Systems (Mamebusv1.0). *Geosci. Model. Dev.* 14, 763–794. doi: 10.5194/gmd-14-763-2021

Nagai, T., Gruber, N., Frenzel, H., Lachkar, Z., McWilliams, J. C, and Plattner, G.-K. (2015). Dominant Role of Eddies and Filaments in the Offshore Transport of Carbon and Nutrients in the California Current Systems. *J. Geophys. Res.: Oceans* 120, 5318–5341. doi: 10.1002/2015JC010889

Ndoye, S., Capet, X., Estrade, P., Sow, B., Dagorne, D., Lazar, A., et al. (2014). SST Patterns and Dynamics of the Southern Senegal-Gambia Upwelling Center. *J. Geophys. Res.: Oceans* 119, 8315–8335. doi: 10.1002/2014jc010242

Nencioli, F., Olmo, G. D, and Quartly, G. D. (2018). Agulhas Ring Transport Efficiency From Combined Satellite Altimetry and Argo Profiles. *J. Geophys. Res.: Oceans* 123, 5874–5888. doi: 10.1029/2018jc013909

Pegliasco, C., Chaigneau, A., and Morrow, R. (2015). Main Eddy Vertical Structures Observed in the Four Major Eastern Boundary Upwelling Systems. *J. Geophys. Res: Oceans* 120, 6008–6033. doi: 10.1002/2015JC010950

Pegliasco, C., Chaigneau, A., Morrow, R., and Dumas, F. (2020). Detection and Tracking of Mesoscale Eddies in the Mediterranean Sea: A Comparison Between the Sea Level Anomaly and the Absolute Dynamic Topography Fields. *Adv. Space Res* 68(2), 401–419. doi: 10.1016/j.asr.2020.03.039

Pelegrí, J. L, and Benazzouz, A. (2015). Coastal Upwelling Off North-West Africa. *Oceanogr. Biol. Features Canary Curr. Large Mar. Ecosyst.* 115, 93–103.

Polito, P. S, and Sato, O. T. (2015). Do Eddies Ride on Rossby Waves? *J. Geophys. Res.: Oceans* 120, 5417–5435. doi: 10.1002/2015jc010737

Richardson, P., and Garzoli, S. (2003). Characteristics of Intermediate Water Flow in the Benguela Current as Measured With RAFOS Floats. *Deep-Sea Res. II* 50, 87–118. doi: 10.1016/S0967-0645(02)00380-6

Rusciano, E., Speich, S., and Ollitrault, M. (2012). Interocean Exchanges and the Spreading of Antarctic Intermediate Water South of Africa. *J. Geophys. Res.: Oceans* 117, 1–21. doi: 10.1029/2012JC008266

Sangrà, P., Auladell, M., Marrero-Díaz, A., Pelegrí, J., Fraile-Nuez, E., Rodríguez-Santana, A., et al. (2007). On the Nature of Oceanic Eddies Shed by the Island of Gran Canaria. *Deep-Sea Res. I* 54, 687–709. doi: 10.1016/j.dsr.2007.02.004

Sangrà, P., Pascual, A., Rodríguez-Santana, Á., Machín, F., Mason, E., McWilliams, J. C., et al. (2009). The Canary Eddy Corridor: A Major Pathway for Long-Lived Eddies in the Subtropical North Atlantic. *Deep Sea Res. Part I: Oceanogr. Res. Papers* 56, 2100–2114. doi: 10.1016/j.dsr.2009.08.008

Sangrà, P., Pelegrí, J. L, Hernández-Guerra, A., Arregui, I., Martín, J. M, Marrero-Díaz, A., et al. (2005). Life History of an Anticyclonic Eddy. *J. Geophys. Res.* 110, 1–19. doi: 10.1029/2004JC002526

Schütte, F., Brandt, P., and Karstensen, J. (2016a). Occurrence and Characteristics of Mesoscale Eddies in the Tropical Northeastern Atlantic Ocean. *Ocean Sci.* 12, 663–685. doi: 10.5194/os-12-663-2016

Schütte, F., Karstensen, J., Krahmann, G., Hauss, H., Fiedler, B., Brandt, P., et al. (2016b). Characterization of 'Dead-Zone' Eddies in the Eastern Tropical North Atlantic. *Biogeosciences* 13, 5865–5881. doi: 10.5194/bg-13-5865-2016

Souza, J. M. A., de Boyer Montégut, C., and Traon, P.-Y. L. (2011). Comparison Between Three Implementations of Automatic Identification Algorithms for the Quantification and Characterization of Mesoscale Eddies in the South Atlantic Ocean. *Ocean Sci.* 7, 317–334. doi: 10.5194/os-7-317-2011

Stegner, A. (2014). Oceanic Island Wake Flows in the Laboratory, in Modeling Atmospheric and Oceanic Flows: Insights From Laboratory Experiments and Numerical Simulations. *Remote Sens. Lett.*, 265–276. doi: 10.13140/2.1.4081.7926

Stegner, A., Vu, B. L, Dumas, F., Ghannami, M. A, Nicolle, A., Durand, C., et al. (2021). Cyclone-Anticyclone Asymmetry of Eddy Detection Ongridded Altimetry Product in the Mediterranean Sea. *J. Geophys. Res.: Oceans* 126, e2021JC017475. doi: 10.1029/2021JC017475

Stevens, B., Bony, S., Farrell, D., Ament, F., Blyth, A., Fairall, C., et al. (2021). EUREC4A. Earth System Science Data 13, 4067–4119. doi: 10.5194/essd-13-4067-2021

Stramma, L., Bange, H. W, Czeschel, R., Lorenzo, A., and Frank, M. (2013). On the Role of Mesoscale Eddies for the Biological Productivity and Biogeochemistry in the Eastern Tropical Pacific Ocean Off Peru. *Biogeosciences* 10, 7293–7306. doi: 10.5194/bg-10-7293-2013

Tian, F., Wu, D., Yuan, L., and Chen, G. (2019). Impacts of the Efficiencies of Identification and Tracking Algorithms on the Statistical Properties of Global Mesoscale Eddies Using Merged Altimeter Data. *Int. J. Remote Sens.* 41, 2835–2860. doi: 10.1080/01431161.2019.1694724

Veitch, J. A., and Penven, P. (2017). The Role of the Agulhas in the Benguela Current System: A Numerical Modeling Approach. *J. Geophys. Res.: Oceans* 122, 3375–3393. doi: 10.1002/2016JC012247

Villar, E., Farrant, G. K, Follows, M., Garczarek, L., Speich, S., Audic, S., et al. (2015). Ocean Plankton. Environmental Characteristics of Agulhas Rings Affect Interocean Plankton Transport. *Science* 348, 1261447–1261447. doi: 10.1126/science.1261447

Wang, Y., Castelao, R. M, and Yuan, Y. (2015). Seasonal Variability of Alongshore Winds and Sea Surface Temperature Fronts in Eastern Boundary Current Systems. *J. Geophys. Res.: Oceans* 120, 2385–2400. doi: 10.1002/2014jc010379

Wang, Y., Liu, J., Liu, H., Lin, P., Yuan, Y., and Chai, F. (2021). Seasonal and Interannual Variability in the Sea Surface Temperature Front in the Eastern Pacific Ocean. *J. Geophys. Res.: Oceans* 126, e2020JC016356. doi: 10.1029/2020jc016356

Wang, Y., Zhang, H.-R., Chai, F., and Yuan, Y. (2018). Impact of Mesoscale Eddies on Chlorophyll Variability Off the Coast of Chile. *PLoS One* 13, e0203598. doi: 10.1371/journal.pone.0203598

Yasuda, I. (1995). Geostrophic Vortex Merger and Streamer Development in the Ocean With Special Reference to the Merger of Kuroshio Warm Core Rings. *J. Phys. Oceanogr.* 25, 979. doi: 10.1175/1520-0485(1995)025<0979:gvmasd>2.0.co;2

Yasuda, I., and Flierl, G. R. (1995). Two-Dimensional Asymmetric Vortex Merger: Contour Dynamics Experiment. *J. Oceanography* 51, 145–170. doi: 10.1007/BF02236522

Conflict of Interest: The authors declare that the research was conducted in the absence of any commercial or financial relationships that could be construed as a potential conflict of interest.

Publisher's Note: All claims expressed in this article are solely those of the authors and do not necessarily represent those of their affiliated organizations, or those of the publisher, the editors and the reviewers. Any product that may be evaluated in this article, or claim that may be made by its manufacturer, is not guaranteed or endorsed by the publisher.